Atomic lifetime measurements employing an electron beam ion trap[1]

E. Träbert

Abstract: Transition probabilities relate to atomic structure and dynamics in ways that are different from straightforward spectra. Besides being a tool for fundamental physics studies, the knowledge of transition probabilities is essential for applications in plasma physics and astrophysics. Techniques and procedures used for measuring the lifetimes of levels in highly charged ions by employing an electron beam ion trap are reviewed to illustrate the state of the art. Examples are drawn from experiments that involve observations in the visible, extreme-ultraviolet, and X-ray ranges, and cover atomic lifetimes in the femtosecond to second range.

PACS Nos.: 32.70.Cs, 32.30.Jc, 32.30.Rj

Résumé : Les probabilités de transition sont reliées à la structure et à la dynamique atomique d'une façon qui est différente des simples spectres. En plus d'être un outil fondamental d'étude en physique, la connaissance des probabilités de transition est essentielle pour les applications en physique des plasmas et en astrophysique. Nous passons en revue les techniques et procédures pour mesurer les temps de vie de niveaux dans des ions hautement chargés, qui utilisent un piège ionique à faisceau d'électrons (EBIT), le dernier cri dans le domaine. Les exemples sont empruntés d'expériences qui utilisent des observations dans le visible, l'ultraviolet et les rayons X, tout en couvrant des temps de vie atomiques allant de la femtoseconde jusqu'à la seconde.

[Traduit par la Rédaction]

1. Introduction

Atomic line spectra reveal atomic structure as well as the fact that energy is quantized. Transitions take place between the "fixed" excitation levels of an atom. However, not all combinations of levels occur in the actual spectra, and spectral lines differ in intensity. These observations can be interpreted by means of selection rules (invoking parity, angular momentum, spin, etc.), and by the concept of transition probability, or the "A factor" A_{ki} for a transition from level k to level i. The mean life τ that appears in the exponential decay law of an excited level is the reciprocal of the sum of all transition probabilities from a given level

$$\tau_k = 1/\Sigma(A_{ki})$$

Although radiative decay properties are often described in terms of a damped oscillator, with the Lorentzian line shape of full width at half maximum (FWHM) (the "natural" line width) directly linked to the "damping", or the decay rate, there is no classical reason for the quantum mechanical atom to decay. Spontaneous radiative decay appears to be understood only in terms of interaction with the fluctuating quantum vacuum, invoking the thought frames of quantum electrodynamics. Because of these fundamental problems or the incomplete understanding of their workings, it has been considered that the decay of atomic levels may not be perfectly described by an exponential decay law (see, for example, refs. 1 and 2); however, there appears to be no clear evidence of nonexponential decay of atomic excitation yet, and we stick to that simple law for the time being.

Atomic lifetime measurements on electric dipole (E1) transitions yield information on atomic wave functions that supplements the insight derived from the atomic energy level structure alone. The E1 transition rate depends on the transition energy and an extra power of r, because the electric dipole operator er explicitly depends on r. Quantum mechanics has found orthogonality requirements for the angular parts of the atomic wave functions, whereas there appears to be no such guiding principle for the radial wave functions. This is one of the reasons why radial wave functions are more difficult to calculate reliably. An imperfect description of the radial wave functions has a larger effect on the E1 transition rates than on the atomic level structure. On the other hand, a good measurement of E1 transition rates (or level lifetimes dominated by E1 decays) yields information on atomic wave functions that supplements the insight gained from atomic energy levels alone. E1 transitions are the "usual type" that dominates most spectra; the opacity and thus the radiation balance of most plasmas is largely determined by E1 transitions. Evidently, it should be valuable to test the reliability of opacity calculations by testing the underlying E1 transition probabilities by selective examples.

Transitions between fine-structure levels of a given term (electric-dipole "forbidden transitions", that is (mostly), magnetic dipole (M1) and electric quadrupole (E2) transitions) are

Received 20 February 2007. Accepted 30 April 2007. Published on the NRC Research Press Web site at http://cjp.nrc.ca/ on 26 January 2008.

E. Träbert. High Temperature and Astrophysics Division, Lawrence Livermore National Laboratory, Livermore, CA 94550-9234, USA (e-mail: trabert1@llnl.gov); Fakultät für Physik und Astronomie, Ruhr-Universität Bochum, D-44780 Bochum, Germany (e-mail: traebert@ep3.rub.de).

[1] Paper given at the Workshop on Twenty Years of Spectroscopy with EBIT held in Berkeley, California, 13–15 November 2006.

 doi: 10.1139/P07-099 © 2008 NRC Canada

supposedly insensitive to imperfectly known radial wave functions, because they connect levels with similar radial wave functions. In the nonrelativistic, single configuration limit, such transitions are supposedly described by rather simple angular coupling factors from Racah algebra (called the line strength S) and the transition energy [3]. However, complex wave functions as well as relativistic effects in highly charged ions modify this simple picture. In practice, theory rarely predicts fine-structure intervals with a precision anywhere near to spectroscopic quality. Therefore, it is customary to replace the calculated transition energies by measured data; the remaining part of the theoretical effort, the line strength, then represents the simple approximation to the line strength modified by the given configuration mix. Recent progress has brought about the first ab initio calculations of such fine-structure transitions that achieve transition energies close enough to experiment so that an eventual correction for experimental data is a minor one (see, for example, ref. 4).

There also are M1 and E2 transitions (as well as the higher multipole orders M2, E3, M3, ...) between levels of different configurations. If low-order multipole decays are available, they will usually dominate, but there are many cases in which low multipole order transitions are forbidden by selection rules for parity and (or) total angular momentum J. Then higher order kicks in, and what may have seemed exotic or negligible otherwise now turns out to provide a dominant process.

Interpreting the level lifetime τ as the time constant of a damped oscillator, there are two ways to measure this parameter. Firstly, by the (Lorentzian) line width, or, secondly, by measuring the line intensity as a function of time and fitting an exponential curve to the data. (The Lorentzian line profile and the exponential decay curve are Fourier transforms of each other.) Classical spectroscopy is hardly sufficient to observe the natural (radiative) line width of levels in neutral atoms that are excited in classical light sources, unless extra broadening mechanisms (like collisions or autoionization — see below) play a major role. Narrow-band laser spectroscopy, however, has achieved this goal. (High multipole order transitions in atoms and low-charge state ions are, of course, required tools for optical frequency standards: Heisenberg's uncertainty principle ties very long level lifetimes — in some practical cases the excited level lifetimes reach years — to very narrow spectral lines.) Also, with (nanosecond)-pulsed laser excitation, it is nowadays quite feasible to selectively excite and then measure the typical nanosecond lifetimes of most low-lying levels of neutral atoms and of some levels of singly charged ions. This option pertains mostly to levels that decay by electric dipole (E1) radiation.

The E1 transition rates of transitions that involve a change of principal quantum number n ($\Delta n \neq 0$) scale as Z^4; for $\Delta n = 0$, the rates scale linearly with Z. High-order multipole transition rates start out very low at low Z, but grow very rapidly, with high powers of Z. For example, the $1s^2\,{}^1\mathrm{S}_0$–$1s2s\,{}^3\mathrm{S}_1$ transition in He-like ions, originates from a purely relativistic effect. In neutral He, the transition rate is so small that the upper level has a lifetime near 6000 s — more than an hour! However, the rate increases with Z^{10}, and in Xe^{52+} ions, the level lifetime is down to a few picoseconds. Experiment has followed this variation over 15 orders of magnitude, with a range of experimental techniques, each tailored to a certain lifetime range. The electron beam ion trap (EBIT) is part of the story and a leading contender for precision in its operating range, as will be explained below. The specific transition mentioned gives rise to the famos line "z" in plasma spectroscopy, and its plasma diagnostic potential depends on its upper level lifetime.

Therefore, for multiply charged ions the level lifetimes are much shorter than for atoms or near-neutral ions. They are out of the reach of lasers, because the laser photon energy is insufficient to reach the excited levels and excite them selectively. Moreover, the decay time usually is too short for classical electronic timing measurements. An alternative is provided by fast ion beams that experience excitation by being passed through a thin foil [5]. The ions in the beam lose a fraction of their energy, but apart from that, the ion beam leaves the foil largely unharmed and continues its trajectory. The distance of the ions from the rear side of the foil translates into time after the end of excitation. Therefore, one can record the spatial decrease of the light intensity emitted by the ion beam as a function of distance from the foil and convert that to a time measurement in the picosecond to many-nanosecond range. Sending the excited ions into a heavy-ion storage ring extends the level lifetime measurement range to the millisecond and even second range.

Atoms and ions with levels that are particularly short-lived (because of autoionization decay channels, or in highly charged ions) may have a natural line width that is larger than the Doppler width and the instrumental line width that are typical for beam-foil spectroscopy. If autoionization is a direct competitor of the radiative decay one observes, then the intensity of the radiative branch and thus the signal rate suffers, of course. Fortunately, there are cases in which only the lower level of a transition autoionizes, whereas the radiative signal benefits from an unbranched radiative decay towards the broadened level. Given the typical autoionization rates of the order of 10^{14} s^{-1}, the typical lifetimes studied in this way are in the range of a few femtoseconds (for examples see refs. 6 and 7).

EBITs intuitively suggest that lifetimes to be studied there would be long (else there would be no need for extended storage). We will discuss how such measurements of long lifetimes in the microsecond to many-millisecond range can be done with EBITs and electronic timing. We will also explain how short lifetimes (again in the femtosecond range) can be addressed by a line-width measurement, and how all these techniques relate to other types of lifetime measurement, for example, by beam-foil spectroscopy. Reviews of measurements of long atomic lifetimes in various types of ion traps have been presented elsewhere [8–11]. Those reviews provide a more comprehensive literature survey than is intended for the present report that focuses on EBITs and their past, present, and future use for atomic lifetime measurements.

2. On the role of radiative rates in plasma and astrophysics

Plasma diagnostics develops and employs techniques that (among other effects) permit the evaluation of light emission or absorption. As most plasmas vary much more slowly than the typical time constants of radiative processes, level lifetimes are

© 2008 NRC Canada

rarely evaluated or directly applied. Instead, absolute line intensities, absorption strengths, or intensity ratios of prominent lines are being measured and interpreted on the basis of collisional-radiative models that imply knowledge of (very many) atomic level lifetimes. Such models, whether of a fluorescent light tube, of planetary nebulae, or of fuel capsules in laser driven fusion experiments, often encompass hundreds or thousands of atomic levels and ten to a hundred thousand transitions, most of which are between high-lying levels. Such transitions are more easily calculated than measured, and individual uncertainties are assumed to be of secondary importance, with many errors expected to average out. However, there usually are some key transitions that involve low-lying levels with a notable level population. Such transitions are what may be observable in either emission or absorption, and such key transitions are worth investigating by experiment, testing the validity of the atomic structure codes, and providing guidance for their improvement. Depending on ion charge, spectral range, and radiative rates, several techniques may be available. EBIT is not the cure-all remedy for all problems, but is a contender for many.

2.1. Plasma density

A coarse grouping of plasmas is by particle density. Since we discuss diagnostics in the context of EBITs, only low-density plasmas are of interest here. However, "low density" is not well-defined. The electron beam particle density in an EBIT is of the order of 10^{11} to 10^{12} cm^{-3}. The electron density in tokamaks is typically of the order of 10^{13-14} cm^{-3}, that in the solar corona maybe ranges from 10^6 to 10^{10} cm^{-3} (flares reaching up to 10^{13} cm^{-3}), that in planetary nebulae may be as low as 10^4 cm^{-3}. If such a vacuum was technically feasible on Earth, there would be almost no matter within the volume of an ion trap. Planetary nebulae or the solar corona make this up by size. The physics of the diagnostics is, of course, largely the same in each type of low-density plasma. What matters is the collision frequency in relation to radiative rates. Depending on the plasma density, different types of radiative transitions have rates that compete with the collision rates and make level populations depend on particle density.

Radiative rates of the order of 1 s^{-1} (level lifetimes of the order of 1 s) imply that a particle experiences similarly low collision frequencies and has a mean free path of the order of 1000 m at room temperature (25 meV). Particles of keV energies are much faster, while highly charged ions have larger cross sections for electron capture and for reactions with other ions. Only ultrahigh vacua (UHV, typically 10^{-9} mbar and better) let highly charged ions survive long enough for accurate measurements to be done, and thus are compatible with lifetime measurements in the millisecond range; lifetimes in the second range need vacua in the 10^{-11} mbar range or better. Such a good vacuum can be reached easily in a cryogenic EBIT, because the vacuum vessel acts as a large cryopump, and this is one of the great advantages over a "warm" (room temperature) EBIT. The other advantage is the higher magnetic field strength available from superconducting magnets. Actually it is not the field strength on its own, but the magnetic compression of the diameter of the electron beam emitted from a gun that sits in a low-field region. In high-Z ions, the radius of the electron orbits scales with $1/Z$, and thus the cross sections for electron collision excitation decrease rapidly (Z^{-2}). Only very tightly squeezed electron beams provide a sufficiently intense electron shower that ionizes atoms faster than they can recapture electrons.

The depths of the absorption features (relative to a radiation continuum) are proportional to the oscillator strength (and thus to the radiative transition probability) and to the layer density between light source and observer. Absorption by a spectral line of low transition probability is weaker and correspondingly affords a larger optical depth than that of a fully (electric-dipole) allowed transition. (There are astrophysical observations in which only the forbidden magnetic dipole line "z" of O VII reaches Earth as an emission line, whereas all others are absorbed by the interstellar medium, which then imprints its own absorption lines on the background continuum [12].) Absorption usually involves ground-state atoms and ions. Otherwise the collisional excitation rate has to be larger than the radiative decay rate, so that a notable level population of the excited level can be reached and maintained, from which then further absorption can take place.

In emission spectroscopy, the decay signal is proportional to the level population and to the transition probability. Absolute emission measurements can determine absolute concentrations of excited ion species, just as absorption measurements can determine concentrations of absorbing species. A short level lifetime corresponds to a strong emission signal that decays away quickly when excitation ends. If the excitation is not sudden and (or) the detection is not time resolved, the time-integrated emission signal will be proportional to the level population and to the branch fraction. The level lifetime then enters only indirectly, via the decays that counteract the excitation rate in establishing the level population.

2.2. Hyperfine-induced decays

Here are a few more examples of long atomic level lifetimes and their role in the interpretation of spectra from low-density plasmas: When at the Livermore SuperEBIT the $2s$–$2p_{3/2}$ decay in the Li-like ion $^{209}Bi^{80+}$ was measured [13], it was hoped that the relative line intensities would help to confirm the suggested line classification. However, the intensity pattern did not match the statistical population expected on the basis of total angular momentum J and nuclear spin I coupling to quantum number F. Apparently the level populations were modified by collision rates that were not so different from the radiative transition rate within the ground state. (A heavy-ion storage ring experiment on the H-like ion $^{209}Bi^{82+}$ has determined a level lifetime of 0.35 ms [14] — a notably long lifetime, indeed, for such a very highly charged ion.) Thus, the moderately high electron density of SuperEBIT was enough to change the level populations by electron collisions before radiative decay could take place. Inverting the problem, the knowledge of the electron density n_e allowed the authors to infer a half life $\tau_{1/2} = 7 \pm 5$ s of the hyperfine component in Bi^{80+}, in comparison to a prediction of 12.3 s.

In multiply charged ions, the present lifetime measurement techniques reach up to radiative lifetimes of many seconds. Interpreting line intensities in a planetary nebula (where particle

© 2008 NRC Canada

densities and thus collision frequencies are very much lower than in any present terrestrial laboratory), Brage et al. [15] have deduced the 20 min lifetime of the $2s2p\,^3P^o_0$ level in the Be-like ion $^{14}N^{3+}$ with a claimed uncertainty of some 30%. The decay of this $J = 0$ level to the $J = 0$ ground state is possible by single photon emission only because of the hyperfine interaction (I will employ HFS as the usual abbreviation of hyperfine structure and hyperfine interaction). HFS couples the $^3P^o_0$ level to a hyperfine sublevel of the $^3P^o_1$ level, which in turn couples to the $^1P^o_1$ singlet level. So the HFS-induced transition rate trails the resonance transition by many orders of magnitude. If the resonance transition is very fast (as in the He-like ions), the associated HFS level lifetime is measurable by beam-foil spectroscopy on fast ion beams (if it falls into the range of picoseconds to nanoseconds); if the resonance transition itself is much slower (as is the case in Be-like or Mg-like ions), the HFS level lifetime will be correspondingly longer and requires different measurement techniques, like ion trapping in an EBIT or a heavy-ion storage ring. Very recent measurements at a heavy-ion storage ring suggest that the calculations of the HFS decay rates in Be-like ions as used in the above analysis may be wrong by about a third [16], or there may be experimental influences that are not yet understood — more and better experiments are needed!

This coupling and decay mechanism, first discussed to explain the intensity of hyperfine lines in the spectrum of atomic mercury [17], has been checked in a number of He-like ions by beam-foil spectroscopic lifetime measurements. It has been exploited in various ways, from the investigation of the general scheme via providing an X-ray monitor to laser-resonance spectroscopy of hyperfine-induced transitions [18], determinations of the very close level interval near a level crossing [19–21], to the aforementioned lifetime determination from modeling assumptions of astrophysical particle densities [15]. A very recent, rather precise, actual lifetime measurement in this hyperfine context has been achieved on Mg-like ions of Cu, at the Heidelberg heavy-ion storage ring TSR[2]. In this experiment, the lifetime of the $3s3p\,^3P^o_2$ level has been measured, and a 10% contribution from a HFS-induced decay to the ground state been found (and this HFS effect itself has been determined with an uncertainty of well below 10%). This ties in with work reported more than 75 years ago by Huff and Houston [22] who discuss high multipole order radiation and report a private communication by Bowen who pointed out that this particular level in neutral Hg — seen in astrophysical objects — must have the HFS-induced decay branch to explain the line intensity. More than 70 years later, at long last, these HFS influences on the decay rates are measurable in ions with a closed K shell, including isotope effects. This has come about a quarter of a century after measuring the HFS-quenched lifetimes in He-like ions, that is, in ions with a K-shell vacancy. (The K-shell vacancy itself does not matter for the hyperfine effect, but it opens a fast $n = 1$–2 decay channel (a resonance transition), and the multistep mixing with the resonance level connects the HFS-induced level decay with the resonance decay rate. The same HFS physics that leads to nanosecond level lifetimes in He-like ions may lead to millisecond lifetimes in Be-like ions, and so on.) The technical progress of vacuum and ion storage now enables the measurement of atomic lifetimes that are 6 to 8 orders of magnitude longer than those that were accessible 30 years ago. This is not only an end to itself, but the ionic systems that can now be studied are of specific interest in various plasmas. (As a side note, the preliminary results of the measurements on Mg-like Cu ions and the $3s3p\,^3P^o_0$ level indicate similar shortcomings in the calculated HFS-induced decay rates as the Be-like ion work mentioned above. Theory needs testing — and EBIT experiments would provide a different environment from heavy-ion storage rings for such complementary measurements!)

[2] E. Träbert, S. Reinhardt, J. Hoffmann, A. Wolf, and P. Indelicato. Manuscript in preparation.

2.3. Line ratios

Another role for level lifetimes is the intercomparison of line intensities with one line originating from a short-lived, the other from a long-lived level. Ideally, the collision frequency in the plasma ought to be in between the two decay rates to make the line intensity ratio depend on particle density. In the one extreme case (low density), both levels can decay radiatively before perturbing collisions occur; in the other, neither radiative decay can compete with the collision rates. Typical cases for such line pairs are the resonance and intercombination lines of two-electron ions (He-like, Be-like, Mg-like ions). The few-picosecond resonance level lifetimes are usually taken from calculations, but the many-picosecond to nanosecond lifetimes of the upper levels of intercombination transitions can often be measured by beam-foil spectroscopy [5]. Such relative line intensities have been extensively applied to the analyses of the UV and EUV spectra of the solar corona or of cool stars [23–27].

The population dynamics of an atomic system in a plasma may depend strongly on the particular properties of a specific high multipole order (non-E1) transition. An example is the $1s2s\,^3S_1$ level in the He-like ions and the role its decay (line "z") plays in the satellite line pattern in the X-ray range [28, 29]. Different classes of transitions with their different orders of magnitude of the transition rates, therefore mark different time scales, and that is just what may be needed for plasma diagnostics or for the interpretation of an astrophysical light source. Transitions of low transition probability (intercombination and E1-"forbidden" lines) have a larger optical depth and thus permit deeper views into plasmas than the observations of allowed transitions that are optically thick. In the ground configurations of multielectron ions there often are levels of rather long lifetimes; the level populations of these levels depend on the ratio of collisions versus radiative transitions, and so do the relative intensities of the decays of higher levels that are excited from specific low-lying levels. If the first step in the ground configuration is rather large (as it is in N- and P-like ions), the relative line intensities are predominantly temperature sensitive; if the energy steps are small (fine-structure intervals inside a term), the regular use lies in density diagnostics [30, 31]. Depending on the actual level lifetimes, the useful density range may be for applications as a diagnostic in tokamaks [32, 33], or the solar corona, planetary nebulae, and the like, naming just a few of the many astrophysical objects that are being studied in the light of forbidden lines [22, 34–36].

© 2008 NRC Canada

2.4. Solar corona

Iron ($Z = 26$) and nickel ($Z = 28$) are the heaviest elements that appear with a relatively high abundance in the Sun. This abundance feature ties to the particular nuclear stability (binding energy per nucleon) of Fe and nearby elements. In the solar corona, emission lines from many ionization stages of Fe are present. In the long-wavelength range (for highly charged ions, this is the visible part of the electromagnetic spectrum), practically all the lines are from electric-dipole forbidden transitions (mostly M1). Some such lines were observed by Suckewer and Hinnov in the Princeton PLT tokamak [37] more than a quarter century ago, and they have served for plasma diagnostics of low-density plasmas since. Particularly prominent in the solar corona are two of these lines that arise in Fe X (λ 6374.6 Å [38]) and Fe XIV (λ 5302.86 Å [38]), respectively. These lines have not only been seen in the spectrum of the Sun where they are known as "the green and the red iron lines" and they have served in coronal hole studies [39], for large-scale temperature diagnostics [40] as well as for polarization measurements etc., but also in symbiotic stars [41], in Seyfert galaxies [42], supernova remnants [43–48], as interstellar absorption lines [49], in a cooling flow cluster [50], and so on.

These two Fe lines, however, are from transitions within the ground states of the respective ions. For a better understanding of the solar corona, its density and temperature distribution, measurements of lines that connect the ground configuration with a variety of excited levels are wanted. Of particular interest are lines that connect to levels of very different lifetimes, because then the line ratios yield information on level populations that are sensitive to density and temperature. Many such transitions correspond to spectral lines in the EUV; for Fe they are in a wavelength range from about 170 to 350 Å. In this range, Feldman (in a survey of line rations that are of particular astrophysical interest) [51] points out three lines of the Ar-like ion Fe^{8+} that originate from $3p^5\,3d$ levels ($^1P^o_1$, $^3P^o_{1,2}$) of very different lifetimes (picoseconds, a few nanoseconds, many nanoseconds). (There also is a very long lived $^3D^o_1$ level.) These lines have been amply observed in the solar corona, and modeling shows that their line ratios should be very useful diagnostic tools. Ten years earlier, Fawcett and Mason [52] argued similarly (including also lines from the $3p^5\,4s$ configuration). Moreover, they point out that reliable oscillator strengths and collisions strengths are necessary to obtain the tools for a line ratio analysis in an environment like that of the solar corona, but that the theoretical results are sensitive to small changes in the eigenvector compositions. In fact, their own calculational results and those of others were pointed out as requiring major software improvements. Feldman mentions that analyses of these lines in the Ar-like ions for a long time disagreed with analyses based on other isoelectronic sequences, and that only a recent calculation by Liedahl [53] that included many more than just the lowest few configurations removed most of the discrepancies. Clearly, as Feldman argues now, 10 years later, reliable laboratory experiments are needed, since theory is still not fully up to the task.

However, no laboratory light source so far has been able to produce these lines under controlled conditions that come even close to coronal conditions, which means ultrahigh vacuum and electron densities far below 10^{12} cm^{-3}. The decay of the shortest lived of these three Fe ion levels is seen in many light sources, the medium lifetime one has been seen in tokamaks and with foil-excited ion beams [54–59], whereas the longest lived $J = 1$ level ($^3D_1$) has been elusive for a long time. Feldman [51] (in this new version of the long-standing quest for line ratios of forbidden lines [30, 31, 60]) therefore calls for EBIT measurements at various electron beam energies on these and other line ratios, so that reference data for the solar atmospheric work can be derived. EBIT can provide practically monoenergetic electron beams at a constant energy or in energy sweeps that simulate a Maxwellian energy distribution [61]. A consistent set of laboratory line ratios obtained under controlled conditions would then provide a versatile, calibrated tool for the interpretation of such line ratios seen in the Sun. EBIT as the arguably best-suited device for the job, however, operates regularly at electron densities or the order of 10^{12} cm^{-3} and thus needs development work to extend its working range to even lower densities.

The Livermore EBIT has already produced some spectra of the desired ions in the EUV wavelength range [62], but not under conditions that are immediately applicable to the present problem. Future spectra can certainly aid in the assignment of many more coronal spectral lines to the various Fe ion charge states. However, the solar EUV spectrum is densely cluttered with spectral lines, and even the EUV spectrum of Fe is very rich in lines so that additional parameters will be needed to disentangle the spectra. For example, various electric-dipole forbidden lines occur that have been given very different wavelength assignments in the literature. The upper levels of these M1, E2, and M2 transitions feature lifetimes in the millisecond range and thus are important corner stones in any proper coronal-modeling effort. Adding time resolution on the millisecond scale to the capability of recording EUV spectra at EBIT will greatly enhance the diagnostic value of the data.

Theory on its own, in contrast, is not able to provide a reliable reference. For example, Feldman [51] points to recent (unpublished) calculations by Bhatia for some predicted line ratios in Fe XX "that fall in between two previous predictions". Unfortunately, when looking at calculations for the aforementioned coronal Fe lines in the visible (Fe X, Fe XIV), such recent calculations by the very same lead author [63, 64] are the odd ones out, deviating markedly from most of the earlier calculations. This might, of course, imply that the older calculations were insufficient, or that theory is so uncertain that "new" means "no better than old, and perhaps worse". (Maybe there are reliable ways for such computations, but then they are not universally applied.) Experiment is called for to find out.

The first experimental lifetime results on these transitions in Fe X and Fe XIV (from a Texas A&M university Kingdon-type (electrostatic) ion trap operated at Reno (Nevada) [65]), however, seemed to be a bit ambiguous, one result falling short of most predictions and the other lifetime value exceeding all of them. A recent measurement at a heavy-ion storage ring, thus using the presently cleanest technique for obtaining millisecond-range level lifetimes of multiply charged ions, of a number of M1 transition rates in Fe X through Fe XIII [66], has shed severe doubt on the reliability of the Kingdon trap work. This

© 2008 NRC Canada

doubt was corroborated by very recent measurements of the M1 transition rate in Fe XIV at the Livermore EBIT [67], which supports most of the earlier calculations. At an experimental uncertainty of as little as 1% the experimental finding is much more meaningful than those calculational results that usually carry uncertainty estimates of the order of 20%. The Livermore EBIT result has very recently been corroborated by work at the Heidelberg EBIT, stated with even higher precision. An earlier version of the Kingdon trap hardware from Texas A&M university has been given to the Jet Propulsion Laboratory (Pasadena). Using that device, a Fe XIV lifetime result in between the Reno and Livermore findings has been reported [68]. Judged by basic physics arguments, both Kingdon trap lifetime results are suffering from underestimated systematic errors.

Similar to the work on Fe, the Livermore EBIT work on transition probabilities of coronal lines in Ar [69] has superseded the earlier, probably faulty work with the Kingdon ion trap [70] using more precise data. Since then, lifetime work at the Heidelberg EBIT has pushed ahead in the quest for high precision, on a single level each of Ar XIV and Fe XIV, in both cases corroborating the Livermore findings. More important than the sheer precision, however, is the high accuracy that has been ascertained by attention to possible sources of systematic error. More details can be found in Sects. 5.2 and 5.3.

The results underline the need for a detailed analysis of key radiative transition probabilities, oscillator strengths, line strengths, and level lifetimes, ion by ion. While in some of the cases covered by the various experiments, calculations have yielded results that agree with the experimental findings, other, seemingly similarly extensive, calculations deviate from this by some 10 to 60%. There is not a single type of calculation yet that treats all atomic systems equally well, and for reliable transition rate data on a given system, experiment is very necessary as a reference marker. After all, the aim of solar coronal modeling is not the production of "an answer" based on whatever input data, but a meaningful answer based on valid, reliable input. This is a field to which EBITs can contribute valuable benchmarks.

3. Experimental techniques

EBITs combine the Penning trap principle with a strong, extremely well-collimated electron beam along the magnetic field (a B field of typically 3 to 8 T), thus also defining an axis of symmetry. The electron beam is compressed by the field, to a diameter of about 70 μm [71] (SuperEBIT; EBIT: 50 μm). The Penning parts of the trap are completed by drift tubes on different potentials that keep ions in the trap volume axially confined. The electron beam serves several purposes: the electrons collisionally ionize atoms from the ambient gas or from a gas flow injected ballistically (for example, a neutral gas stream of a density corresponding to a pressure of as low as 10^{-10} mbar that may be crossing the electron beam trajectory under UHV conditions ($< 10^{-11}$ mbar), or the atomic plume ablated from a target under high-power pulsed-laser irradiation), or low-charge ions injected along the magnetic field lines from an external MeVVA ion source. These freshly produced ions are then confined by the trap fields and can be hit by fast electrons over and over again. If the electron–ion collisions are sufficiently frequent (that is why the electron beam needs to be so tightly focused) and energetic, stepwise ionization to ever higher charge states can proceed. This process is moderated by the interplay of ionization, recombination, and charge-changing collisions with the residual gas (this determines the need for ultrahigh vacuum (UHV)). The charge state limit is given by the electron energy and the increasingly high ionization potentials of highly charged ions. The second job of the electron beam is a compensation of the space charge of the cloud of positive ions that is being built up in the trap. Even with a strong magnetic field for radial confinement, the ions would repel each other and move away from the location of the electron beam, if the attractive potential of the beam electrons and the space charge compensation were absent. Indeed, when the electron beam is switched off, as is the case in most of the atomic lifetime measurements discussed below, the trapped ion cloud expands radially by a substantial amount, to a few millimetres. This expansion has been measured by FT-ICR techniques at Livermore; it has more recently been visualized at the National Institute of Standards and Technology (NIST) EBIT [72].

There are basically two ways to measure atomic lifetimes in an EBIT. The first technique employs a steady-state trapped ion cloud for high-resolution spectral observations (discussed immediately below). The second technique makes use of a modulation of the electron beam energy and (or) electron beam current and will be discussed in the section on "magnetic trapping".

3.1. Line width measurements on E1 transitions

In the aforementioned beam-foil observation of radiative decays of autoionizing levels, the signal rate often is poor, because of the poor branching ratios (fluorescence yields). Next, the shape and the width of these weak lines have to be measured, correcting for contributions to the width by instrumental effects. It is then no surprise that the lifetime results from such line-broadening measurements may bear error bars of 10%, 30%, and sometimes even more. This is to be compared to a scatter of the lifetime predictions of autoionizing states that often is an order of magnitude for such levels (which may be "almost" degenerate with continuum levels). The calculations involve the tracking of the outgoing electron from small to very large distances. We find some of the same problems in the measurements at the EBIT. The determination of very short atomic lifetimes via a determination of the line width has not reached the accuracy of a precision tool yet, but it provides insight into EBIT physics besides an interesting estimate of an atomic property.

The basic idea (described in the 1930s by Weisskopf and Wigner [73], in the 1950s by Heitler [74], and since then by Cowan [75] and Griem [76] in their text books) equates the excited level lifetime with the time uncertainty in Heisenberg's uncertainty principle, expressed as $\Delta E \cdot \Delta t \leq h/2\pi$, where ΔE is the excited level width that contributes to the line width of any decay.

In any observation, the line width is not purely the natural one, but a combination of instrumental, thermal (Doppler profile), and natural contributions. To separate the various influences, the line shapes have to be analyzed well. Line broadenings dominated by statistical fluctuations, by Doppler broadening, or by the instrumental line width may be approximated by a

© 2008 NRC Canada

Gaussian profile. In the search for the line-width contribution of the finite atomic level lifetime, this particular line profile would be inappropriate: for such a line, the proper shape is a Voigt profile, with maybe a Gaussian-dominated center, but also with Lorentzian wings that are essential for the very determination of the natural line width part. A Voigt profile can be fitted reliably to these wings only if the signal-to-background ratio is sufficiently high in the range where the wings show, that is, away from the bright part of the line profile. Subsumed in the Gaussian part are the true instrumental line widths of the X-ray spectrometer and any Doppler broadening of the emission from the stored ion cloud. (By the way, having been brought up on the long-standing notion that a Voigt profile cannot be represented analytically, there is a claim that the Voigt profile function has now been expressed exactly [77], and there also is a counter claim that this derivation is faulty [78].)

For a practical experiment, the best situation is with groups of lines some of which represent the decays of long-lived levels and some that arise from short-lived ones. Such a situation occurs in Ne-like ions with $2p^6$–$2p^5\,3s$, $3d$ resonance and intercombination decays, or with the $1s^2$–$1s2p$ ("w", "x", "y") and $1s^2$–$1s2s$ ("z", all in Gabriel's notation [28]) transitions in He-like ions. The line profiles of the narrower ones of these lines represent the instrumental and thermal effects, but suffer only negligible lifetime broadening; they can be fitted by Gaussians. The lines from "fast decays" comprise that one other ingredient, but now in a notable amount, a Lorentzian profile that represents the lifetime broadening. Fitting a Voigt profile to such a line ought to reproduce the Gaussian width of the neighboring lines as a consistency check, because instrumental effects and ion temperature must be the same for both lines; the FWHM of the Lorentzian part of the Voigt profile is directly related to the upper level lifetime.

In the pioneering experiment on this topic [79], Cs ($Z = 55$) was introduced into EBIT as a vapor through a ballistic gas injector. Ions were trapped, charged up to the charge state of interest (Cs^{45+}), and excited. Under trapping and excitation conditions that maximized the signal, the crystal spectrometer line width of the decay of a short-lived $3d$ level appeared to be rather similar to that of a long-lived $3s$ level in the same ion. Evidently, instrumental and thermal (Doppler) contributions to the line width exceeded the natural lifetime contribution. Only when the ion trap was made very shallow (by reducing the potential difference between the drift tubes to very low values or even to zero) so that evaporative cooling was encouraged, and when ion heating was minimized by lowering the electron beam current and thus the number of ions in the trap, the ion temperature and thus the line widths went down [80–82] and by their differences revealed the lifetime differences between the upper levels ($3s$ and $3d$) of the transitions observed in Cs^{45+}.

Similarly to this Ne-like ion species, Graf et al. [83] evaluated EBIT measurements of the He-like ion Fe^{24+}. Here, the resonance line "w" was investigated in comparison with the M2 intercombination line "x" and the M1 forbidden line "z". In the Fe experiment, the natural line width part of lines "x" and "z" was negligible, so that a pure Doppler profile provided a good approximation of the overall line shapes. Only with the much shorter lived upper level of the "w" line was a Lorentzian detected and fitted. Both evaluation paths lead to lifetime results that agree with each other within the error bars, but the weighted mean (1.08 fs, with an uncertainty of about 5%) differs from predictions (2.19 fs [84]) by almost exactly a factor of two.

It is not yet clear in this case whether theory or experiment, or both, needs to be improved. It is intriguing, however, to consider the importance to physics of finding out. For transitions between shells in low-Z atoms and ions, and for intrashell decays along long isoelectronic sequences, experiment has indicated which calculations are good. When modeling plasma spectra, however, the relative line intensities of the $n = 1$–2 transitions in He-like ions (which involve excitation to and transitions between hundreds and thousands of higher lying levels) regularly are not perfectly matched. This has led to the suspicion that the E1 intercombination decay rate (line "y") might be at fault, but beam-foil spectroscopy has measured these rates up to about $Z = 16$ and did not find any discrepancy with the better calculations. Measurements on line "z" have been performed over an extremely wide range of nuclear charges; the most precise data among these measurements are from heavy-ion storage rings and EBIT (see discussion below), and they indicate that theory is well developed. The line width measurements seem to be the only handle on the E1 decay rate of line "w" — and here we have that mysterious mismatch. One of the points that require further study is the actual line shape used in the comparison. It may be that the assumption of a Gaussian shape for the lower rate decay is not quite appropriate, and that a Voigt profile is needed here, too. That, in turn, requires high statistical reliability even outside the apparent line profile, out to the wings that need to be distinguished from the background.

For the sake of completeness: Lifetimes of the same order of magnitude, in the femtosecond range, have also been measured by a very different technique. In beam-foil spectroscopy, the fast ion beams are being passed through a thin (a few hundred atomic layers) foil. The time inside the foil is of the order of a few dozen femtoseconds. In this time, inner-shell ionization can occur, and the X-ray yield depends on the foil thickness and the lifetimes of the K-shell vacancies, the latter being in the femtosecond range. By varing the foil thickness, the K-shell vacancy lifetimes can be determined [85].

3.2. Magnetic trapping

All other atomic lifetime measurements in this report concern long-lived levels. These levels are so long-lived that if the ions were not confined in the trap, they would move away from the production zone and the field of view of the detection apparatus within a fraction of their excited state lifetime, and thus be lost to observation. At thermal energies, ions typically travel about 10 cm/ms, and at the typical ion energies inside EBIT, which are in the keV range, the travel distance is of the order of 10 m. Thus, trapping is a necessity for, both, production by successive electron–ion collisions, and efficient detection. Such lifetimes in the range microseconds–seconds have the advantage, however, of being measurable by electronic timing. The art of the experiment lies in the need to assure that either the excited ions be kept perfectly isolated from any detrimental influences during the measurement, so that the signal truly reflects the entity of interest, or the influences be understood and be under suffi-

© 2008 NRC Canada

ciently tight control so as to minimize the ensuing systematic errors. Systematic error control is, indeed, the decisive issue that marks the progress from some radio-frequency and Kingdon ion trap atomic lifetime measurements via early EBIT work to the present stage of what is possible at an EBIT (see below).

For lifetime measurements that follow the decrease of the emission signal after the excitation stops, two approaches have been tried. In the first, the electron beam energy is modulated above and below the production and (or) excitation threshold [86]. In this way, the ion cloud is minimally perturbed, because the electron beam is present at all times, and thus EBIT runs in its "electronic trapping" mode [87]. However, to avoid complications that are possibly arising from interactions of the ion cloud with the electron beam (for example, by recombination), the electron beam can be shut off completely. This then is the "magnetic trapping" mode [87] in which EBIT acts as a Penning trap. The ion cloud does expand somewhat when the electron beam is switched off, but trapping is still effective for many seconds (as has been ascertained by ion cyclotron resonance frequency observations at LLNL) [87, 88]. This operational mode has become the standard technique for lifetime measurements in the range from a few microseconds to many milliseconds. Most of the further examples discussed below use this technique — except for some work at Heidelberg, where it is found to be beneficial if a weak, low-energy electron beam is maintained even during the "off" periods of the electron beam needed for excitation.

4. Instrumentation

4.1. UV / vis Spectrometer / Stovepipe

The first optical lifetime measurements using an EBIT were reported from the NIST EBIT [89, 90] (using the same technique — but now for transitions in the visible — that had already been tested for X-ray observations in the course of the Livermore work [87] that proved the validity of the magnetic trapping mode). There, visible-range light from the trap was collected and made parallel by a large aperture ratio lens, transported away from EBIT, and focused onto the entrance slit of a grating monochromator. For spectral observations, the monochromator was tuned to different wavelengths; for lifetime measurements, the monochromator was set to match a desired spectral line, and then the signal of the photomultiplier at the exit slit was recorded as a function of time in a cycle that alternated between ion trapping with the electron beam on and off (electronic and magnetic trapping modes as dubbed at Livermore [87]). The set-up demonstrated that the arrangement was able to yield meaningful lifetime data.

At Livermore, a spectrometer for the visible and UV ranges and a transmission grating spectrograph for the near ultraviolet are available [91, 92], but with their time-integrating charge-coupled device (CCD) camera detectors, these two devices have been employed for spectroscopy only. For the Livermore EBIT lifetime experiments in the visible and near-UV spectral ranges, instead of using a monochromator, an interference filter was inserted into the light path. The resulting "Stovepipe" instrument (Figs. 1 and 2) has been described elsewhere [94]. Although this is a somewhat less flexible approach (most lines need their individual special filter), the light yield has been excellent. The high statistical quality of the data soon showed the need for a better understanding of the systematics; the ion loss due to charge exchange was recognized as a major source of systematic error for atomic lifetime measurements in the millisecond range. Benefiting from these improvements, two of the three NIST EBIT lifetime measurements were revised considerably (the third seems alright within its 7% uncertainty, but that should be improved upon), and the lifetimes of many other levels were measured for the first time [69, 93, 95–97]. A direct comparison with a measurement of the same ion in a heavy-ion storage ring [98] demonstrated that both measurements suffer from different systematics, but can yield coincident, reliable results, if the systematic effects are properly corrected for.

The Freiburg (later Heidelberg) EBIT group has opted for a monochromator for visible-light observations. Since their electron beam (and therefore also the axis of the ion trap) is horizontal, while the entrance slit to the spectrometer is vertical, the 90° rotation of the image of the trap is achieved by several reflections in between ion trap and spectrometer. The spectrometer at Heidelberg is much more powerful than the one at NIST Gaithersburg. Demonstrating the high spectral resolution, the

Fig. 1. Schematics of optical lifetime experiments at the Livermore electron beam ion trap using the Stovepipe set-up. Reprinted with permission from ref. 93. Copyright 2003 American Institute of Physics.

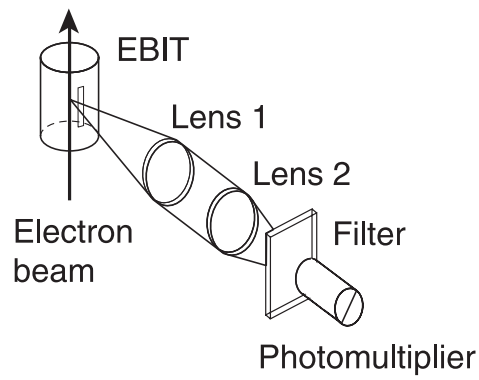

Fig. 2. Stovepipe signal: Timing pattern of a measurement with the Stovepipe spectrometer. Reprinted with permission from ref. 93. Copyright 2003 American Institute of Physics.

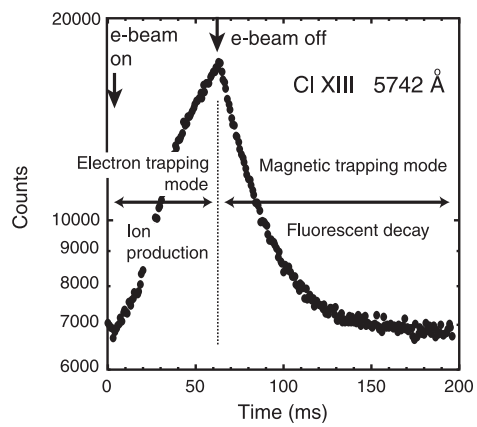

© 2008 NRC Canada

Fig. 3. Line strengths of transitions in the ground term of B- and F-like ions as measured at an electrostatic ion trap (EST), a heavy-ion storage ring (TSR), and various EBITs (at NIST Gaithersburg, Livermore (LLNL), and Heidelberg (HD)). The nonrelativistic expectation for the line strength in both systems is the Racah algebra factor 4/3. The upper horizontal line in the upper part indicates the theoretical expectation after introducing the quantum electrodynamics correction because of the electron anomalous magnetic moment [101].

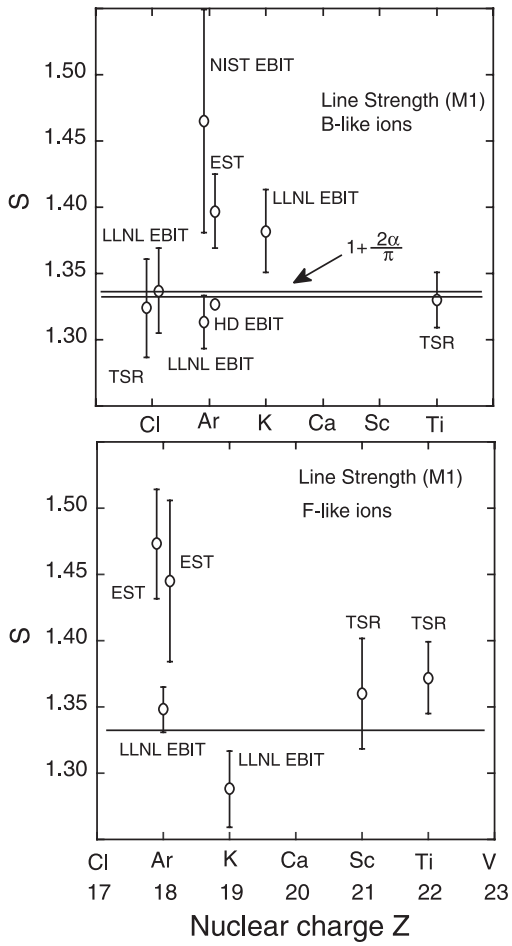

Zeeman splitting of lines in the 8 T magnetic field of the Heidelberg EBIT has been observed [99]. In terms of wavelength accuracy, highly accurate measurements of M1 lines of various argon ions have been reported [100]. The same instrument, with a photomultiplier serving as the detector, has also been used for lifetime measurements, in particular on M1 lines of Ar and Fe, as will be discussed in Sects. 5.2 and 5.3.

Lifetime data on M1 decays in Be-, B-, and F-like ions have by now been obtained at electrostatic ion traps, at various EBITs, and at the Heidelberg heavy-ion storage ring. An intercomparison of the data and a comparison of the data with the results of calculations (which are considered to be fairly reliable in these relatively simple cases) is best done on a line strength scale, because it removes the energy scaling of the transition rate; the rates vary by about a factor of two between neighboring ions, or by a factor of 30 from Cl ($Z = 17$) to Ti ($Z = 22$), whereas the line strength S is practically constant (see Fig. 3). Such a comparison (see the time line in Fig. 4)

Fig. 4. Time line of lifetime measurements on the M1/E2 transition in the ground term of the B-like spectrum Ar XIV. The vertical line represents the latest calculations by Volotka et al. [101]. Older calculation scatter within about 0.6% near this mark.

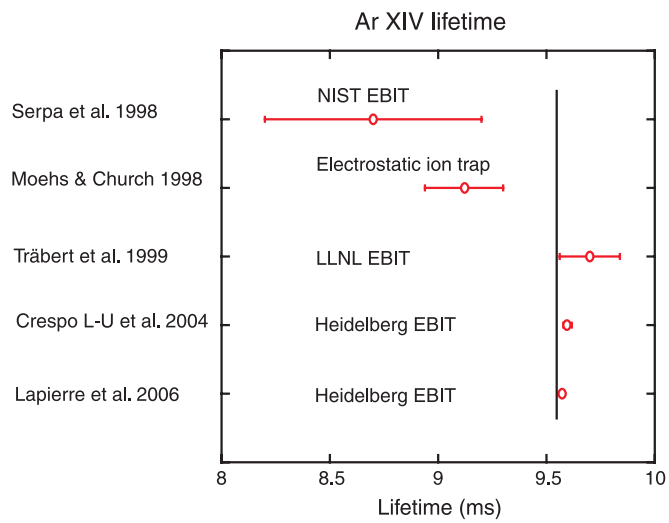

indicates that in the early electrostatic ion trap [70, 102, 103] and NIST EBIT [90] measurements, the errors must have been underestimated, whereas EBIT work at Oxford [104], Livermore [69, 96, 98], and Heidelberg [105–107] as well as the storage ring work [98, 108, 109] has yielded consistent results. The recent measurement of the M1/E2 transition rate in B-like Ar XIV [106, 107] carries an error bar of less than 0.1%. At this precision, the result means a new challenge to theory (see Sect. 5.2).

At the same time, claiming such accuracy requires the experimenters to do the testing of the technique to such a high level. For lifetime measurements in the 1% accuracy range, for example, the clocks built in to PCs are clearly good enough (typical specifications are 10^{-5}). Because frequency generators need occasional recalibration, a better time reference is needed somewhere. One option are atomic clocks that have come down in size and price. The LLNL EBIT laboratory has opted for a Loran C receiver instead; the Loran system was originally developed for long-range navigation where the position information depends on the time differences of signals from long-wavelength radio transmitters. The transmitters nowadays are coupled to atomic clocks, and thus one can (relatively cheaply) remotely lock a receiver to atomic clocks that are being provided by government laboratories.

A larger problem is caused by the problem of the finite ion storage time as a substantial correction to the apparent lifetime as determined by exponential fits to the decay curves. Time-resolving detectors for visible light (photomultiplier tubes) have a dark rate that corresponds to thermal noise and cosmic radiation releasing electrons from the photocathode. Only the thermal noise can be reduced by cooling; the actual noise signal cannot be electronically discriminated from the true photon signal. This dark rate is present also in the decay curves, and it dominates after the true radiative decay has (exponentially) lost most of its intensity. However, at low rates, it is difficult to distinguish the dark rate from a structured background signal

© 2008 NRC Canada

Fig. 5. Decay curves of Ne extracted from time-resolved X-ray spectra. Upper curve: At an electron beam energy of 3 keV, neon atoms can be fully ionized. The decay curve at the position of the M1 line in He-like Ne^{8+} shows a tail that we associate with recombination of Ne^{9+} ions. Ne^{9+} ions are produced by ionization of Ne^{8+} ions (as long as the electron beam is on) and by recombination of Ne^{10+} ions. Reprinted with permission from ref. 111 Copyright 1999 American Physical Society.

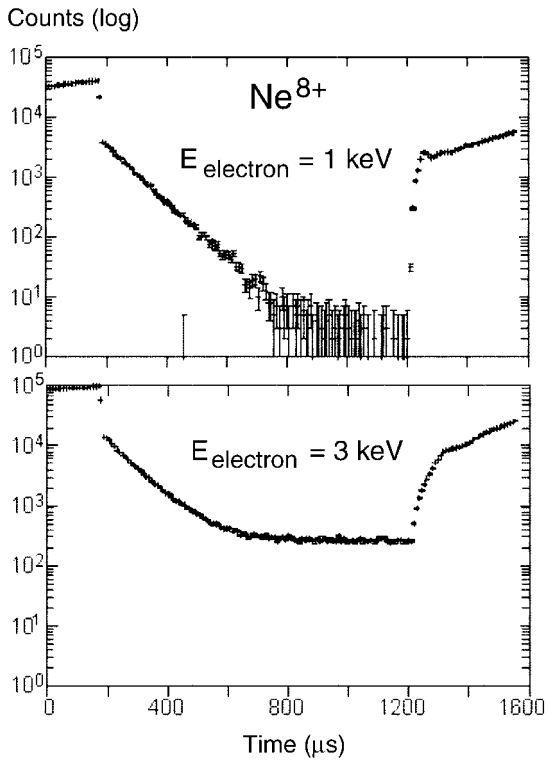

that might depend on EBIT operations and the trapping cycle. This problem is common to all detectors, and I will return to this point in Subsect. 4.4 on ion loss measurements and charge exchange.

4.2. X-ray diodes

Practically each EBIT set-up is equipped with an X-ray diode for monitoring the ions in the trap. Such solid-state detectors (Si(Li) or intrinsic Ge (IGLET)) detectors offer a large solid angle and a good X-ray detection efficiency. Spectra from such detectors are of sufficient resolution to derive a rough charge state balance, and to detect characteristic emission from certain ionization stages of heavy ions (for example, H-like, He-like, Ne-like ions). With the trap operated in a cyclic mode, X-ray signal counts can be time stamped [110] and thus sorted by both energy and time into two-dimensional spectra. Cuts along the time axis can be extracted as decay curves, while cuts along the energy axis yield information about possible line blends. The signals of such energy-dispersive devices can be well discriminated against noise.

In contrast to the excitation process in beam-foil spectroscopy, the electron beam in an EBIT does not excite ions from the ground state to high-lying, high angular momentum levels. If nevertheless a decay curve should feature a tail (which may lead to systematic errors in the lifetime determination, see Fig. 5), then this usually indicates the presence of repopulation by charge exchange (CX) with the (electrically neutral) residual gas particles. Consequently it is wise not to produce ions in charge states higher than the one of interest, if it can be avoided [112].

Early Livermore EBIT decay curve measurements on He-like ions — the M1 decay of the lowest triplet level, $1s2s\,^3S_1$, is of particular interest in astrophysics and plasma physics — have used a beam energy modulation technique in which the electron beam energy was periodically lifted above and dropped below the threshold for reaching the level of interest [86, 113]. Since then, it has been found that it is not necessary for continued ion trapping to maintain the electron beam, and the latter has been switched on and off fully ever since [87, 111, 114, 115]. By fast switching techniques, the Livermore measurements have reached the nanosecond lifetime range (on S [116] and in unpublished work on Ar), whereas at low nuclear charge Z the measured lifetimes reached into the millisecond range. With error bars down to 0.5%, the (published) results are in excellent agreement with the trend of lifetime data (at lower Z) from the Heidelberg storage ring, and with extensive nonrelativistic (but relativistically corrected) and some fully relativistic calculations [84, 117, 118] (Fig. 6). As has been mentioned in the introduction, this He isoelectronic sequence is one of the longest that has been studied by experiment (with level lifetimes varying over 15 orders of magnitude). More atomic physics details will be discussed in Sect. 5.1.

In terms of meaningfully small errors, we note that the storage ring and EBIT lifetime measurements in their ranges of applicability have single-percent errors, whereas the techniques that are available in the other ranges of nuclear charges (very long and rather short lifetimes) have typical errors rather in the 10% range.

4.3. Microcalorimeter

In recent years, microcalorimeters have entered the stage of X-ray detection. Working by different principles and material combinations, they all involve small material samples (much below 1 mm^3) at very low temperatures, well below 0.1 K. Measuring the heat from the absorption of an X-ray photon in such a small physical pixel, however, permits energy dispersive spectroscopy at a spectral resolution that, while not as good as that of a crystal spectrometer, is much superior to a classical solid state X-ray detector. Present-day microcalorimeters have line widths below 10 eV for X-ray energies of 0.5 to 20 keV, and, to increase the detection solid angle, they are mounted in arrays. Pixel arrays offer the additional benefit of revealing cosmic rays, because those usually affect more than one pixel. If the data storage occurs with time-stamped events, then filtering routines that identify (near-) coincident events in various pixels can clean up spectra quite notably, making some 10% of the apparent counts "disappear" in favor of those that relate to the object in view.

The electron beam ion trap usually operates in a cyclic mode, with the time per cycle chosen to accommodate the breeding time of a given charge state of interest and the time the ions are to be interrogated or observed. The data are then best stored in time bins that correspond to the phases of the trapping cycle. From such time-sorted counts one can construct time-resolved spectra (breed phase, electron beam on, electron beam off, etc.). With

© 2008 NRC Canada

Fig. 6. Isoelectronic data He sequence: Iso-electronic trend of the transition rate data for the $1s^2\,{}^1S_0$–$1s2s\,{}^3S_1$ magnetic dipole (M1) transition in He-like ions. The level lifetimes range from more than 1 h for neutral He atoms to a few picoseconds for He-like Xe^{52+} ions, and the lifetimes require different techniques for measurement. Data points for $Z = 4$ to 7 are from the Heidelberg heavy-ion storage ring TSR, data for $Z = 7$ to 16 have been obtained at the Livermore EBIT-II [111, 113–116] (with lifetimes ranging from several milliseconds to hundreds of nanoseconds). Data on heavier ions are from the use of (mostly fast) ion beams. All experimental data have been scaled by normalization to the results of the fully relativistic calculation by Johnson et al. [84], and only the deviations from this prediction are displayed.

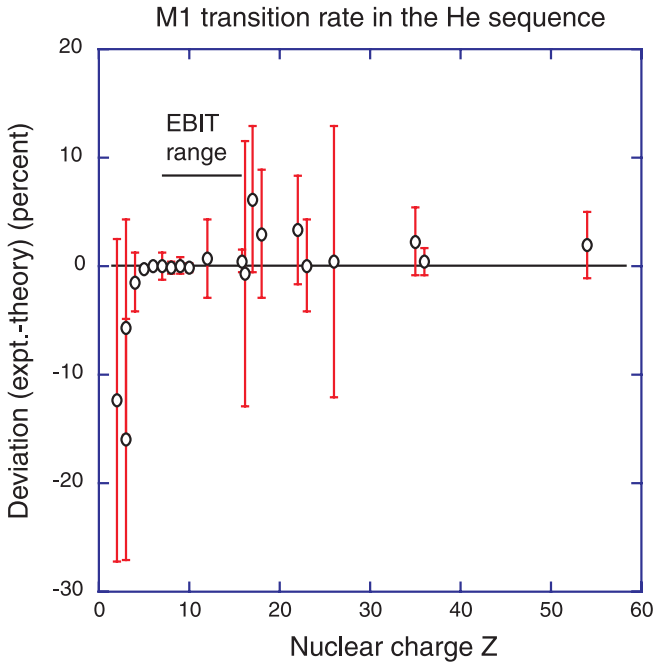

Ni-like Xe^{26+} ions, such a procedure has been demonstrated, using a Goddard-built XRS microcalorimeter [119, 120] that has 32 pixels (of which about half were used, limited by the available signal electronics). Figure 7 shows a scatter plot of a Livermore experiment with Xe, at an electron beam energy of 1500 eV. The pulse height of each signal event is interpreted via a suitable calibration as a photon energy (vertical axis) and placed in the trap cycle according to its time stamp. The aim of this experiment was the Ni-like ion of Xe, that is, Xe^{26+}. Ni-like ions have a metastable level that decays only by a magnetic octupole (M3) transition, and the rate for this high-multipole-order decay is low. The lifetime of this level is in the range of several milliseconds. All other transitions that contribute to the soft-X-ray spectra of Xe^{26+} represent level lifetimes in the microsecond to femtosecond range. Events within energy bands in the scatter plot can be projected onto the time axis and thus be converted to decay curves.

For only a few energies, there are events that occur after the electron beam is switched off. Two drastically different examples — from the same data set — are shown in Fig. 8. The fast (sub-nanosecond) decay in H-like oxygen is followed by a flat, elevated background that we ascribe to CX in which bare oxygen ions capture an electron from the residual gas. In contrast,

Fig. 7. Scatter plot of a measurement of Xe using the XRS microcalorimeter at the Livermore EBIT. Reprinted with permission from ref. 121. Copyright 2006 American Physical Society.

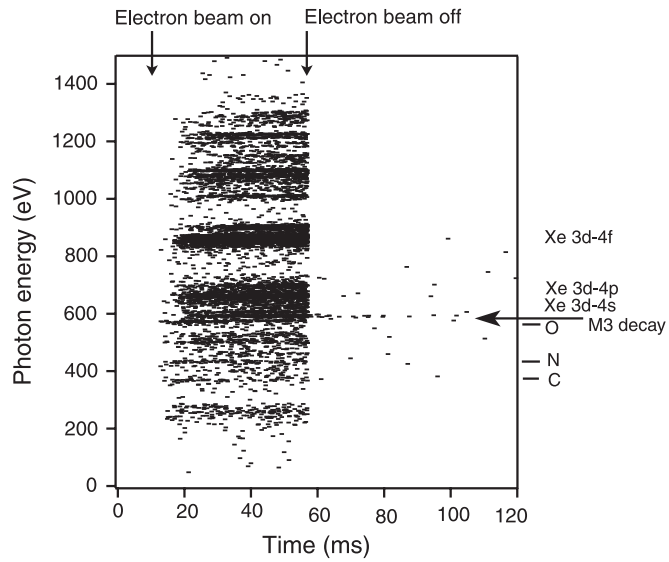

at a single other photon energy of about 590 eV, the projection reveals an exponential decay with a level lifetime of about 11.5 ms. This is the decay that we ascribe to the $3d^9 4s\,{}^3D_3$ level in the Ni-like Xe ion.

This metastable level at an energy that is about half as high as the ionization potential provides a population trap and a stepping stone for ionization of the Ni-like ion well below its regular ionization threshold. Knowing the level lifetime helps in the proper modeling of the charge balance. At the Livermore EBIT the lifetime was measured for three Ni-like ions, of Xe, Cs, and Ba [121]. The lifetimes follow a parallel to the predicted isoelectronic trend. At the time, all calculations predicted longer lifetimes than were measured, by some 30 to 50%, and theory as well as experiment were neglecting the role of hyperfine interaction. For more details, and a resolution of the systematic discrepancy with the calculations, see Sect. 5.5.

The M3 decay is the only one that shows a discernible decay curve in the time-resolved microcalorimeter data. However, the He- and H-like oxygen ions (from CO_2 injected for wavelength calibration) also show delayed photon signals at the positions of the resonance transitions. Their radiative decays are much faster than the time resolution of the microcalorimeter; what causes the flat curve tail is not the lifetime of some bound state, but charge exchange of bare and single electron oxygen ions with neutral particles of the residual gas, followed by radiative de-excitation.

4.4. Ion-loss measurements and charge exchange

In all atomic lifetime measurements using ion traps, it is of paramount importance to determine the ion storage time (the inverse of the loss rate). The observed optical signal decay rates represent the sum of the true atomic decay rate and of all other loss processes, notably the loss of ions from the stored sample. Only when the loss rates are known, can the radiative transition rate be determined from the apparent decay rate. This task is

© 2008 NRC Canada

Fig. 8. Signal curves of two lines of Xe XXVII and O VIII, respectively, within the full trap cycle. Both curves have been extracted from microcalorimeter data like those shown in Fig. 7. After the fast atomic decay, the lower curve is practically flat, but the signal is at an elevated level compared to the background at other photon energies. This is a signature of the CX process in which bare O ions capture an electron from residual gas particles. The upper curve shows an exponential decay, which is identified with the M3 decay of the metastable level in Ni-like Xe ions. Adapted from ref. 121. Original figure copyright 2006 American Physical Society.

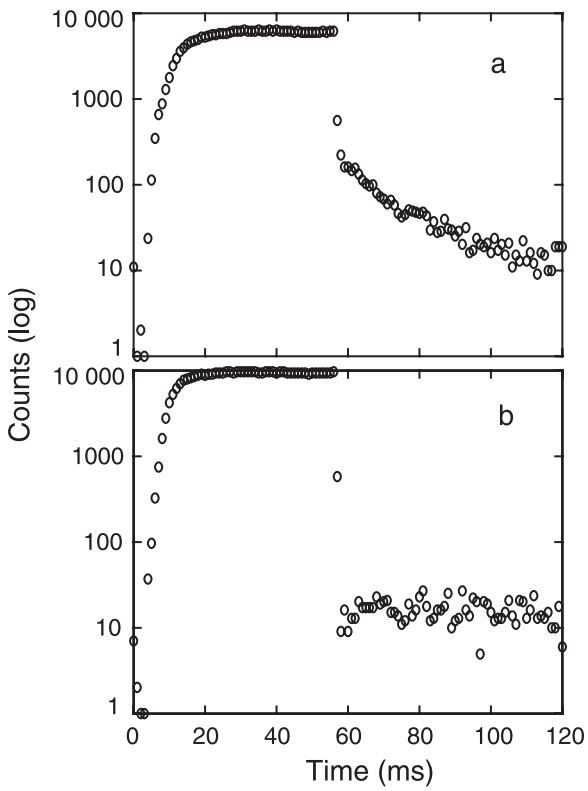

most easily dealt with in heavy-ion storage rings, where only ions of a single charge state are being stored, so that a measure of the change of ion beam current is at the same time a measure of the change of ion number.

In an EBIT, in contrast, ions of several species (elements and charge states) usually are stored at the same time. If by a collision with a residual gas atom a stored ion gains an electron (or more), it may well remain trapped. In this way, there can be both losses of the charge state species of interest as well as gains resulting from the recombination of more highly charged ions. Examples of the latter effect have been shown in lifetime experiments on He-like Ne ions [112]. In those experiments, the decay curves had a massive tail when the electron beam was high enough to produce the next higher charge state ions as well, which could then recombine. Although the signal rate was much higher when the electron beam current could be run higher because of the higher beam energy, this mode turned out to not only suffer from that recombination tail, but also from a slight, but important systematic change of the apparent lifetime in the primary decay component (Fig. 5). Evidently, it is best to have the charge state of interest as the highest one produced (which can be regulated by the electron beam energy).

Another loss mechanism is ion evaporation from the trap along the magnetic field lines. Making the trap deeper (higher drift tube voltages) would seemingly raise the barriers, however, in a shallower trap (after evaporation of the fastest ions), the ion cloud is less hot and also better confined. There is the compromise that the trap at the end of the ion breeding period (when the heating electron beam is switched off) can be made deeper. The Heidelberg EBIT group reports that such ion loss is practically nonexistant for drift tube voltage differences of 500 V or higher [107]. Ions can also collide with other ions and with neutral atoms of the residual gas. In both cases, electron transfer (charge exchange CX) is possible, and the trajectories can change so that a drift of the highly charged ions across the magnetic field lines should be possible. Last, but not necessarily least, the space charge of the ion cloud may trap a corresponding number of electrons, as may happen in pockets of the external fields that form the trap [107].

Although the Livermore and Heidelberg EBIT groups have investigated a number of systematic errors and have thus improved the reliability of such atomic lifetime measurements enormously, the problems are not yet fully solved, as in particular the examples in Sect. 5.2 will demonstrate. A key problem is the fact that typical decay curves show a tail that has a much longer characteristic time (smaller time constant) than the decay of interest; depending on the interpretation of this tail, it can and must be used to correct the apparent lifetime of the primary decay component, or it is hardly related to this problem. Thus, the error budget of any accurate lifetime measurement hinges on the understanding of this feature. Moreover, there are various practical problems. If the slow-decay component matters, it has to be established concurrently (or under very similar conditions) with the actual decay curve measurements. However, measuring a 10 ms radiative decay and a 5 s tail in the same trap cycle results in a frighteningly poor duty cycle for the primary decay signal as well as in complications with the choice of time resolution, channel numbers, and so on. In a fast trap cycle (of, say, 100 to 150 ms for the above example), the tail may be monitored, but its slope cannot be determined reliably. So separate measurements of the principal decay constant and of the decay curve tail will usually be necessary.

When the magnetic trapping mode was explored [87, 88], it was established that the storage time of highly charged ions in a proper (clean UHV) EBIT can be longer than 5 s and may even reach minutes. Such time scales are accessible by ion cyclotron motion techniques and by X-ray observations with a large solid angle detector. The latter benefits from the fact that typical X-ray events in a solid state detector can be well-discriminated against the electronic noise, so that even very low-count rates can be established with confidence. Unfortunately, in many atomic systems that one wants to study for the lifetimes of long-lived levels in the ground configuration (of principal quantum number $n = 2$ or 3), the K shell is closed, and there are no X rays that a large X-ray diode would detect. Transitions into the ground configuration then would likely fall into the soft-X-ray or EUV wavelength bands, for which no energy-dispersive detectors are available, while wavelength-dispersive detection systems offer

© 2008 NRC Canada

only small solid angles and low detection efficiency — too low, in fact, for a practical monitor of radiation from CX events.

If under such circumstances one wants to use X rays as a monitor for CX rates, one has to obtain them from ion species different from the species one is interested in, and then transfer the information gained from that species to the one of interest, via theoretical estimates of the cross sections. The collisional cross sections of ground-state one- or two-electron ions with residual gas particles may be considered sufficiently well-known, but the corresponding cross sections of excited many-electron ions (on which the actual lifetime measurements are done) are not. At present only estimates can be made. One of these is based on the observation that the CX cross sections at the low collision energies of present concern vary linearly or quadratically with the ion charge (or with some power of the ionic charge in between); simple scaling then interconnects the CX loss rate of more highly charged ions with that of the lower charge states of primary interest for a given atomic lifetime measurement. It is not clear, however, whether the charge scaling may be transferred from K-shell ions to, say, L-shell ions. As long as the CX ion loss rates are several orders of magnitude lower than the atomic transition rates to be measured, the uncertainty of the scaling process affects the lifetime measurements only at the level of a few percent or less. This may be of little importance for the interpretation of astrophysical data, which often suffer from many other, larger uncertainties. In the quest for testing the accuracy of extensive calculations, however, errors of this magnitude are possibly decisive.

If CX plays a role, it must be more important when the vacuum is not as good as can be. This has been investigated in various experiments at, both, a heavy-ion storage ring [108] (by switching off part of the pumps) and EBITs (by increasing the gas injection pressure). For example, in the Livermore EBIT experiments on B-like Cl [98], the gas injection pressure was varied by several orders of magnitude (from less than 10^{-8} Torr (1 Torr = 133.322 Pa) to more than 10^{-6} Torr), which leads to an estimated pressure range in the actual gas plume between 10^{-10} Torr and about 10^{-8} Torr. The apparent atomic lifetime was considerably shorter (of order 10%) at the higher pressure than under good vacuum conditions. When the electron beam energy was raised to produce He-like ions, a CX-related X-ray signal at those high injection pressures showed up. The X-ray-based CX ion loss rates were then applied to correct the apparent decay rates seen in the optical measurements. Subtraction of the CX rates from the apparent optical decay rates yielded an approximation to the desired atomic decay rates. In the better vacuum range, the results were constant and consistent with the data from the heavy-ion storage ring. Even the poor-vacuum data came close to the good-vacuum data after correction for CX losses, and, therefore, it seems clear that CX processes play a role and need to be taken into account. If, however, the Heidelberg EBIT group claims that in their experiments CX is found to be unimportant, this is to be understood as work in a very good vacuum range, after testing for such systematics. On the other hand, there have been lifetime measurements at the NIST EBIT [90] in which much higher electron beam energies (of order 15 keV) were found to be useful in producing much more signal than at the beam energy (about 1 keV) that "on paper" should have been sufficient to produce ions of the right charge state. This raises the suspicion that the vacuum was not as good as one might hope for. (The vacuum gauges are mounted to the UHV vessel in convenient places; nobody has yet found a way to actually measure the vacuum where it matters, that is inside the ion trap. The vacuum differences discussed here are in a pressure range that is hardly accessible to gauges, and gauges for the UHV are rarely calibrated at that. So intercomparisons from one laboratory to the other are difficult — except by the physics results.) The lifetime results on Ar and Kr fell short of what later Livermore experiments under better-controlled conditions found, and no correction for CX was done, because this was not recognized as necessary at NIST at the time. Thus, in hindsight, one may be able to understand why certain experiments yielded deficient lifetime results. By the way, the short-falling Ar result from the NIST EBIT was in the good company of electrostatic ion trap results obtained by the Texas A&M group [65, 70, 102] (see Fig. 4), which apparently also suffers from significant underestimates of systematic errors.

After the Livermore experience with ion-loss time constants corresponding to many seconds (and to less than a second under dire vacuum conditions), it came as a surprise when the HD EBIT group claimed [105] that they had such good control over their experiment that they experienced "no losses" at all, as long as the trap depth was of the order of 1 kV. The claim was based on variations in the voltage pattern on their many-element drift tube assembly and on the initial step that many decay curves show at the time when the electron beam is being switched off. If one has no such losses, then, of course, one does not have to correct for them. If …

Especially it was claimed that the CX rates were so low that CX processes were unimportant for the accuracy of the lifetime determination, since they had no notable influence on the ion confinement. A slow component of the decay curve was instead blamed on the role of free low-energy electrons. The peak signal-to-tail ratio of the Livermore and Heidelberg decay curve data is rather similar. However, the Heidelberg group finds that the ratio depends on the background pressure (in the very good UHV range) and on whether the electron beam is being switched off completely or only in part, with the lowest tail signal achieved for low, but nonzero residual beam currents. Therefore, the Heidelberg group finds it advantageous to not shut down the electron beam completely, but to provide a low-energy low-current beam even in the data taking period after ion production and excitation by a strong electron beam have ended; the weak beam supposedly helps to heat low-energy electrons and ions and thus remove them from the trap [106, 107] (which they make deeper than was the case of the Livermore experiments [69]). The production of supposedly free electrons of low energy that show in the slow tail of the decay curves at Heidelberg is blamed on details of the electron-beam switching process; the Heidelberg experiments are interpreted to show the smallest electron beam leftovers if the electron beam is reduced by switching off only the acceleration voltage, whereas a simultaneous defocusing (to achieve faster switching times in the trap) is found to be detrimental. The free electrons may be bound to the ion cloud by the space charge, or be trapped in incidental potential troughs of the drift tube structure. Accord-

© 2008 NRC Canada

ing to the Heidelberg interpretation, these low-energy electrons are available to excite the stored ions to the long-lived, few-eV excitation levels within the ground configuration that is being studied in their lifetime experiments. The electron reservoir is long-lasting; the Heidelberg group finds a slope of this tail that indicates a lifetime of order 1 s. There is no direct observation of these low-energy trapped "free" electrons, however.

Another part of the data on which discussions about systematics hinge is the background level in decay curves. Obviously, a low dark-rate detector should permit a high contrast between signal and background. The contrast in the comparable measurements on, say, Ar XIV is about the same at Livermore and at Heidelberg. However, at Livermore, the background is suspected to be slightly sloped, whereas the Heidelberg group reports a practically flat background. Livermore claims that the changing load on the electron gun, which is being switched on and off, contributes to the slope of the optical signal (via stray light from the gun's glow), and different running conditions have supported this idea. However, even when individual runs had excellent data statistics, the results of subsequent runs have scattered more than was expected from the apparent statistical reliability of the individual data sets, which does indicate the presence of unrecognized effects.

This evidently is a rich field for speculation with only limited experimental access, but it is necessary to pursue the systematics to reduce the uncertainties. Measurements that yield "useful data" are long since feasible, but the other challenge is to test theory at high levels of accuracy. For such tests, Livermore, for example, plans to provide several observation channels that operate in parallel, capturing line and background information separately but simultaneously. For basic physics, the geometry of the electron beam furthermore suggests doing polarization studies of the excitation process. Last, but not least, the possible influence of the magnetic field of the EBIT on the lifetime of some levels should not be overlooked. The strong field destroys the spherical symmetry of the Coulomb field, and thus levels that are forbidden to decay by specific selection rules in a Coulomb potential may do so in the presence of perturbations. An example is the lowest excited $J = 0$ level in Ne-like Ar [122] that does decay by a single photon decay in the presence of a magnetic field. The relative line intensity may be developed into a plasma diagnostic tool [123], and level lifetime measurements at different field strengths might help to test the underlying theory.

5. Examples

Looking at the physics and the data, and trying to make out an ordering scheme for atomic lifetime measurements using EBIT that befits a review, turns out to be a challenge. There are the applications aspects in plasma and astrophysics, the interplay of calculations and measurements, and the physicists' general experience that the challenge of higher accuracy often has led to new fundamental physics insight, and in this case it also touches on new questions.

Having discussed electric dipole transitions and their role in opacity above, the remainder of this presentation will turn to long level lifetimes, that are roughly in the time range from microseconds to seconds. The transitions are all "electric-dipole forbidden" ones, that is, in increasing multipole order of the expansion of the radiation field, there are magnetic dipole (M1), electric quadrupole (E2), magnetic quadrupole (M2), electric octupole (E3; used in the development of atomic clocks, but not presently covered in EBIT), and magnetic octupole (M3) transitions. At low nuclear charges, these transitions have a very small probability, which is why in our everyday environment the atomic spectra are dominated by the much more probable E1 transitions. The E1-forbidden transitions, however, scale with high powers of the nuclear charge Z, and in the "upper half" of the table of the elements, these transitions are quite comparable in rate and intensity to E1 transitions.

Our atomic lifetime interest with EBIT is somewhere in between, in the range where the time constants of these non-E1 transitions are still small (but not vanishingly so) and very different from those of E1 transitions, so that the associated lines may depend on the environmental conditions (temperature, density) of a low-density plasma. To serve as reliable plasma diagnostic tools, collisional-radiative calculations ought to refer to reliable atomic parameters, of which we here are concerned with radiative rates. Of course, where the occasion arises, a physicist tries to find out whether one can do better than the minimum requirement of data quality for a given application. Some of the data discussed below consequently are only as good as the development and testing of the experimental technique and a given applications context warranted. In other cases, the needs of any practical application have long since been fulfilled, but the quest now is on for finding out the limits of the technique, and of our physics understanding of the processes involved. Reviews of the various atomic lifetime measurements that also cover other ion trap techniques can be found elsewhere [9–11].

5.1. M1 transitions in He-like ions

In the mid-1940s, Breit and Teller [124] developed calculations showing that the lowest triplet level, $1s2s\ ^3S_1$, in heliumlike ions ought to decay predominantly by a multiphoton process, which would be difficult to identify in experimental spectra. Nevertheless, several decades later, graduate student Carole Jordan dared to identify a feature in the X-ray spectrum of the Sun with the single-photon decay of this level in He-like Ar [125]. New calculations by various people then corroborated that the single-photon process should be dominant by far, and a Z^{10} dependence of the transition rate was agreed upon after some initial uncertainty, assuming that the transition is brought about by a purely relativistic operator. By now this transition probability and the He isoelectronic sequence have been measured from neutral He (level lifetime of about 6000 s) to Xe^{52+} (with a lifetime of a few picoseconds). The spectral line in question is, of course, the by now the well-known plasma physics line "z". An early precision calculation of the transition rate, by Drake [117], with extensive nonrelativistic wave functions and a relativistic operator, has been supplemented by a relativistic correction determined by Lin [118]; no less than 25 years later a fully relativistic treatment, by Johnson et al. [84], has at long last matched the low-Z accuracy of the earlier calculation and extended it to high values of Z.

© 2008 NRC Canada

Table 1. Atomic lifetime measurement results of electron beam ion trap (EBIT) experiments on the M1 transition in He-like ions. All of these measurements have been done at Livermore (LLNL EBIT), observing the M1 decay in the X-ray range.

Ion	Level	Lifetime τ	Ref.
He sequence			
N^{5+}	$1s2s\ ^3S_1$	(3.92 ± 0.13) ms	87
		(3.94 ± 0.05) ms	115
O^{6+}	$1s2s\ ^3S_1$	(956 ± 5) μs	114
F^{7+}	$1s2s\ ^3S_1$	(274 ± 3) μs	115
Ne^{8+}	$1s2s\ ^3S_1$	(90.5 ± 1.5) μs	86
		(91.7 ± 0.4) μs	111
Mg^{10+}	$1s2s\ ^3S_1$	(13.61 ± 0.49) μs	113
S^{14+}	$1s2s\ ^3S_1$	(703 ± 4) ns	116

Early experiments aimed at the lowest members of the isoelectronic sequence (with typical errors of about 10%), and at ions from $Z = 16$ upwards (lifetimes in the hundreds-of-nanosecond range and shorter). The latter work was mostly done by beam-foil spectroscopy, with typical error bars of 5 to 10%. The smaller uncertainties reported in some of those measurements are not beyond doubt. Then dielectronic recombination (DR) measurements at a heavy-ion storage ring [126, 127] on B, C, and N ($Z = 5$–7) produced lifetimes in the millisecond range, with uncertainties below 1%. Not much later, the magnetic-trapping mode of electron beam ion traps was explored at the Livermore EBIT, with X-ray observations of He-like N ions [87]. The observation required no more than using the X-ray diode that observes EBIT anyway, which was now to be run by time stamping the signal events in relation to the phase of the EBIT trap cycles. This cyclic variation incorporated the production of the proper ion and population of the level of interest by employing an electron beam energy above the excitation energy of the level of interest, but below the next higher levels. Then the electron beam energy was dropped below the excitation threshold, and the decay of the X-ray signal monitored. After a while the trap was emptied and a new cycle began.

The same measurement technique, maintaining the electron beam, but modulating the beam energy, was used for He-like Ne [86] and Mg [113]. In a further step, the electron beam was shut off completely, in measurements on O [114], S [116], N and F [115], and again Ne [111] (Table 1). The second-generation Ne [111] experiments were done in two settings. In one setting the signal was maximized by running a high electron beam current that was available at an energy much higher (3 keV) than necessary to produce the charge state of interest. In the other setting, the electron beam energy (1 keV) was chosen so as not to produce any ions more highly charged than Ne^{8+}, and correspondingly a high decay curve tail ascribed to recombination was present only in the first setting (see Fig. 5). The lower beam energy and lower signal rate data also yielded a lifetime value that slightly, but significantly, differed from that obtained in the brute force setting. Only this result from the cleaner experiment agreed with the good predictions. It was then realized that the good calculations in this case differ by much less than the experimental error bars, and that experimental tests discriminating between these calculations are not in present reach. The situation can then be interpreted differently: Experiment can use the comparison with theory (in this case of a special transition in He-like ions) as a proof of validity of the measurement scheme; only experiments that meet this yardstick can be expected to obtain reliable lifetime results in other cases (that theory cannot be relied upon to produce). EBIT measurements can reach this precision and accuracy. Measurement techniques that do not meet this criterion should be suspect.

The accuracy of the measurements improved over time to better than 0.5%. The EBIT measurements on this atomic system are listed in Table 1 and included in Fig. 6. The recently published data for S^{14+} (with a lifetime near 700 ns [116]) are fully compatible with the theoretical trend, whereas the unpublished Livermore results for Ar^{16+} (also obtained by Crespo López-Urrutia et al.) do not — a 200 ns atomic lifetime might have been stretching the experimental capabilities by too much, possibly because the drift tube structure is not optimized for such fast-timing experiments.

5.2. M1 transitions in few-electron ions

There are E1-forbidden transitions in the ground configurations of ions with several (at least five) electrons. Actually, in B-like ions and F-like ions, the atomic structure is particularly simple, and only a single transition each (mostly M1, with a subpercent E2 contribution) appears. This transition then gives rise to a line with particularly low excitation energy that can serve as a marker for the presence of an ion species in a given charge state and thus serve as a temperature diagnostic. Once the ion is produced, the line ratios of lines connecting with the two ground configuration levels may serve for density diagnostics [128].

These simple cases have long since been identified with lines in the solar corona and in the spectra of low-density terrestrial plasmas. Because of their simplicity, they have also been treated numerously by theory, and the transition-rate predictions appear to scatter only by about 0.5%. This fine agreement, however, is deceptive. According to basic atomic structure theory, the transition probabilities of such transitions between fine-structure levels of the same term, at least in the nonrelativistic limit, can be expressed by the line strength, a factor that describes atomic wave function geometry, and (some power of) the transition energy. The transition energy can be determined by spectroscopic observation to a much higher accuracy than by typical calculations. Hence, it is customary to compare the result of transition energy calculations with experiment, and — finding insufficient agreement — to replace the calculated value by the measured one. The line strength can be obtained from Racah algebra and (in the nonrelativistic limit, single-configuration picture) is a simple fraction. It turns out that the good mutual agreement of the various published calculations for the M1 (E2) transition rates in the simple few-electron systems (like the previously mentioned B- and F-like ions) arises from "semi-empirically adjusted" transition energies and from line strengths that must not vary too far from the Racah algebraic values. In fact, for all practical purposes, the straightforward recipe calls for a combination of experimental energies with the plain Racah factors.

© 2008 NRC Canada

The first EBIT observation of such M1 transitions was achieved at Livermore [129]. In the case of Ar and some other elements, the first actual transition rate measurements of this type of transition were performed using an electrostatic ion trap [70, 102] or using the NIST EBIT [90]. The results of these experiments, however, did not come particularly close to the range of the aforementioned prediction, and it is evident meanwhile that those experiments must have had shortcomings in the assessment of systematic errors. At the Livermore EBIT the experimental conditions were varied over a wide range to learn about systematic errors, and the only error source found to offer mismatches as large as seen with the deviant data was a massive worsening of the vacuum in combination with a lack of control over the ion storage time.

Away from the nonrelativistic limit, and in the usual situation of multiconfiguration wave functions, simple rules fail, and detailed theory is needed (but it still regularly employs that "semi-empirical adjustment" to experimental energies). However, a calculational scheme that does not satisfactorily deal with the simple case must be suspect when being applied to more complex situations. On the other hand, if theory — traditionally quoting some 10 to 20% uncertainty on M1 transition rates in rather simple cases — by intercomparison of various calculations seems to do much better when judged by the scatter of the predictions (in simple cases!), then the experiment is challenged to find out how good theoretical predictions actually are. Hence, there is quite a bit of interest in testing lifetime predictions to a much higher precision than is needed in any present application. At a heavy-ion storage ring, such a test has been achieved a lifetime uncertainty of only 0.13% on the intercombination decay in C^{2+} [130], the most accurate such value on any multiply charged ion at the time and way ahead of theory. Eventually, this result incited a massive calculational exercise [131] that involved several hundred thousand configurations and yielded an intercombination transition rate with the unprecedented accuracy of about 0.5%, and this theoretical result and the experimental data point disagree by slightly more than their combined error bars. Similarly, resonance transitions in neutral rare-gas atoms are challenging theory at their sub-one-percent uncertainties. So what and how well can EBITs do in this context, and with truly highly charged ions?

The most promising case for an attempt at precision is the M1 transition in B-like Ar^{13+} (spectrum Ar XIV), with a wavelength (4412.4 Å) [100] that is in the blue range of the visible spectrum and very favorable for efficient light detection by a low-noise bi-alkali or tri-alkali photomultiplier. The basic detection arrangement is shown in Fig. 1 for the Livermore stovepipe experiment. A pair of lenses image the center of the trap onto a photomultiplier far enough away from the EBIT (about 1 m) so as not to suffer from stray magnetic fields. A suitable bandpass filter (or a monochromator) selects light from the line and its spectral neighborhood. The time history of such a light signal is shown in Fig. 2. Obviously, a monochromator permits the selection of any wavelength in its wavelength range, but it may have an overall lower transmission than a filter. A filter may have a narrow band pass, but the bandpass of an affordable standard filter is not necessarily centered on the line of interest, and will usually include some background. Such background contributions may arise from ions in the trap, scattered light from vacuum gauges, the hot filament of the electron gun in the EBIT, or from surfaces or residual gas particles struck by ions or electrons, possibly with transients when switching the electron beam off. The thermal emission from the electron gun changes when the electron beam current is being varied, and the time constant of those thermal changes can be close to the atomic rates. Evidently, it is desirable to find out about those background light contributions, to minimize and to quantify them. Because some systematic error source might vary with parameters beyond those available for a given ion species, experiments carried out on several ions along an isoelectronic sequence [69, 96, 98], on B-, F-, and Be-like ions (the latter has an M1 transition in an excited configuration) have been checked against EBIT data from other EBIT laboratories [104], and checked against results from other reliable techniques like, for example, the heavy-ion storage ring [98, 108, 109]. The validity of the basic technique has thus been ascertained, but there certainly is room for further improvement, with particular interest in the reduction of experimental error.

In the Livermore experiments, the statistical reliability of the individual data sets was very high, but for as yet unidentified reasons, the lifetime values extracted from the decay curves varied from run to run. In contrast, the Heidelberg EBIT group (5 years later) claims almost perfect reproducibility. They present an Ar XIV lifetime with an error bar that is a small fraction of 1%. Such small uncertainties actually challenge atomic structure theory. Most of the calculations of the M1/E2 transition rate in the B-like ions (see refs. 101, 132–137, for example) scatter by about 0.6% even after adjusting to experimental transition energies. Evidently, the new lifetime data with their extraordinarily small error bars challenge the way calculations have been done so far.

New calculations have been solicited [101] that include a variety of previously neglected effects like specific QED terms [106, 107]. For example, the calculations that have been done in response to the Heidelberg measurements include the electron anomalous magnetic moment (EAMM) [101], which would seem to represent an improvement over simpler approximations. This contribution amounts to about 0.5% in this case. Because this correction alone is almost as large as the scatter of the earlier calculations, it is no surprise that it is not clear whether among them is a preferable one. It has even been discussed whether to use the anomalous magnetic moment of a free electron instead of that for the bound one, but such a thought seems moot, as the electron is bound. There are other aspects that merit closer inspection instead. For example, nowadays one can safely assume that the QED part of such calculations (and this includes the EAMM correction) can be computed sufficiently well. Problems remain, however, with the computer implementation of classical quantum mechanics, in quite a number of atomic structure calculations. This may explain the scatter of the predictions noted above.

The extremely precise Heidelberg lifetime result on Ar XIV is slightly longer than the value expected from a basic combination of the well-known transition energy (also measured with unprecedented precision at the Heidelberg EBIT [100]) and the simple line strength ($S = 4/3$). QED corrections usually af-

© 2008 NRC Canada

Table 2. Atomic lifetime results of electron beam ion traps (EBITs) measurements on few-electron ions with E1-forbidden decays (mostly M1 with a weak E2 admixture). The measurements were done at Gaithersburg (NIST), Heidelberg (HD), Livermore (LLNL), and Oxford.

Ion	Level	Lifetime τ	Trap	Ref.	Comment
Be sequence					
Ar^{14+}	$2s2p\,^3P^o_2$	(15.0 ± 0.7) ms	Oxford EBIT	104	594 nm M1(M2)
		(15.0 ± 0.8) ms	LLNL EBIT	69	
K^{15+}	$2s2p\,^3P^o_2$	(7.6 ± 0.5) ms	LLNL EBIT	96	464 nm M1(M2)
B sequence					
Cl^{12+}	$2s^22p\,^2P^o_{3/2}$	(21.0 ± 0.5) ms	LLNL EBIT	98	574 nm M1(E2)
Ar^{13+}	$2s^22p\,^2P^o_{3/2}$	(8.7 ± 0.5) ms	NIST EBIT	90	441 nm M1(E2)
		(9.70 ± 0.15) ms	LLNL EBIT	69	
		(9.597 ± 0.021) ms	HD EBIT	105	
		9.573(4)(5) ms	HD EBIT	106	
		9.573(4)(+12 −5) ms	HD EBIT	107	
K^{14+}	$2s^22p\,^2P^o_{3/2}$	(4.47 ± 0.10) ms	LLNL EBIT	96	345 nm M1(E2)
F sequence					
Ar^{9+}	$2s^22p^5\,^2P^o_{1/2}$	(9.32 ± 0.12) ms	LLNL EBIT	69	553 nm M1(E2)
K^{10+}	$2s^22p^5\,^2P^o_{1/2}$	(4.44 ± 0.10) ms	LLNL EBIT	96	426 nm M1(E2)

fect only energy splittings, and such a contribution would be straightforward to apply. Since the transition energy is known from experiment, there is no basis for an energy correction to matter. However, the EAMM affects the transition operator, and therefore the situation is different and, in a way, more interesting. According to theoreticians involved in the above theoretical treatment, the M1 transition in a B-like ion, the case of our example, and thus the level lifetime, is to change by a QED factor of $(1 - 2\alpha/\pi)$, which amounts to about 0.5%. The EAMM as a basic QED contribution suggests that a general correction should be applicable to all such decays. However, no systematic treatment has been reported yet on corrections to transitions of other multipole order (E2, M2, M3) decays, nor on how these corrections scale with the nuclear charge or the principal quantum number (as the usual QED energy corrections do).

A similar EAMM correction, as predicted for B-like Ar, might worsen the agreement of basic theory and measurement for several other ions (Al-like, Cl-like) for which uncertainties of less than 1% have been achieved in experiments at a heavy-ion storage ring [138, 139]. However, not only are the sizes of the corresponding EAMM corrections not yet known — in most cases there is no quantum mechanical (non-QED) calculation available yet that might be sufficiently accurate and precise to test the EAMM effect. The theory of atomic transition probabilities has rarely been challenged to deliver such high accuracy before. (The struggle about resonance line transition probabilities in Li and Na, and the quest for a fully relativistic treatment of the M1 transition in He-like ions have lasted for about a quarter century each!) Measurements on Fe XIV at the Livermore EBIT [67] have been corroborated at Heidelberg, with a result that agrees well with calculation without the EAMM, and the experimental uncertainty of the result ($16.726^{+0.020}_{-0.010}$ ms [140]) is about as small as in the Heidelberg measurements of Ar XIV. It should be noted that both of the extremely precise Heidelberg lifetime results are slightly longer than theory predicts, whereas typical systematic errors of ion trap experiments tend to result in lifetime data on the short side.

The EBIT lifetime data on few-electron ions are listed in Table 2.

5.3. M1 and M2 transitions in many-electron ions

B- and F-like ions have an open $n = 2$ shell; rather similar (with an open $n = 3$ shell) are the Al- and Cl-like ions, also featuring a single prominent M1 transition each. Because Fe is such an abundant element, and the solar coronal temperature range is favorable, the forbidden lines in Al-like Fe XIV and Cl-like Fe X are rather prominent in the spectrum of the solar corona. The other Fe ions with an open $3d$ shell also have E1-forbidden transitions in their more complex ground configurations or in the $3d$ shell. The combination of easy production of ions in an EBIT because of the higher ionization potential with the favorable shorter wavelength has led to measurements on Fe XIV at the Livermore EBIT Laboratory. The other $3p$-shell Fe and Fe-group ions have largely been covered in measurements at a heavy-ion storage ring [138, 139, 141–143], superseding most earlier results from other ion traps.

A Livermore EBIT study of the green corona line (Al-like Fe XIV) was the first optical EBIT lifetime measurement that produced a result with an uncertainty of less than 1% [67]. (The same basic considerations as concern calculations, transition energies, and line strengths apply as in the aforementioned case of B-like ions.) This result superceded the systematically offset value found in an experiment using an electrostatic ion trap [65]. It possibly also ended a long string of calculations of the astrophysically important transition rate that could not provide this number except by using the experimental transition energy.

The LLNL EBIT decay curve obtained on the transition of interest in Fe XIV is of high quality; after correction for the

© 2008 NRC Canada

ion storage time that was seen as limited by CX processes, a lifetime value of (16.74 ± 0.12) ms was derived, that is, with an uncertainty of less than 1%. (I have already mentioned the even more precise most recent lifetime measurement of the same level at the Heidelberg EBIT [140].) Figure 9 illustrates the interest in this transition and its transition rate by presenting a time line of calculational and measurement results. Most calculations feature results that more or less agree with that of the LLNL EBIT measurement. However, most of these calculations have been "semi-empirically adjusted", and thus they ought to show the same results as one gets from combining the experimental transition energy with a given Racah factor line strength. The few deviant theoretical results have not been adjusted and thus demonstrate the (poor) true state of the respective calculations. Only very recently, the first ab initio calculations have been performed that yield the proper answer without the fudging process [144]. As mentioned earlier, another Kingdon ion trap experiment [68] (at JPL), that is with a trap of the same type as used in the Reno work, has reported a lifetime closer to the Livermore and Heidelberg EBIT results than that first one from an electrostatic ion trap [65], but it does not agree with (rather firm) theory — in contrast to the EBIT data.

The corresponding graph for Fe X (not yet measured with good accuracy at EBIT — the ionization potential of only 262 eV is rather low) has a similar story to tell [143], only in that case the deviation of the earlier electrostatic ion trap measurement by Moehs and Church [65] has a different sign. (One is tempted to say that the systematic errors of the electrostatic ion trap technique for highly charged ions are insufficiently understood, and the results are not even reliably wrong. The scatter so far is much larger than the quoted uncertainties. Of course, not all EBIT lifetime work has been reliable either, but with increasing insight, the learning curve plateau has been reached quickly.)

EBIT measurements of atomic lifetimes of the order of 10 ms go along with trap cycle times (ion production and excitation, observation with the electron beam off, and purging the trap) of the order of 150 to 200 ms. Such rapid cycling is best done with gas injection, using a ballistic gas injector that has a reservoir pressure of 10^{-9} to 10^{-7} mbar and injects a gas plume of central pressure 10^{-11} to 10^{-9} mbar into a trap region with surfaces at liquid He temperature and thus probably of 10^{-13} mbar residual gas pressure. An obvious candidate gas for heavier ion species than Ar is Kr, which may eventually be used as a radiation blanket in large fusion devices like the International Thermonuclear Experimental Reactor (ITER). At the Livermore EBIT, several long-lived levels in highly charged Kr have been studied for their lifetime, by observing decays in which visible light is emitted. Several levels showed lifetimes that were at odds with calculations that covered M1 and E2 transitions, but not the M2 decay branches. Including the latter into the calculations changed the specific lifetime predictions by up to 50% and brought about satisfactory agreement of calculation and measurement.

Figure 10 shows an example of transitions in P-like ions. There are heavy-ion storage ring results for iron group elements and LLNL EBIT data for Kr, each device in its favorable working range. Figure 10 shows a variety of lifetime predictions by their deviation from the eventual measured values. Several recent calculations come close to what has been found in the experiment. Most earlier calculations feature a grossly deviant isoelectronic trend; their results might agree with measurement for one ion or two (if any), but not for many others. The transitions used in the example are not exotic — the decays are of the two lowest excited levels in the ground configuration of P-like ions.

This experience reflects similar occurrences elsewhere; the usual atomic structure calculation packages contain options that users switch off to save computation time or output file length — at the cost of lack of physics completeness. Just as those M2 decays in (for example, Ar-like) Kr [97], there are long-lived $3d$ levels in Fe ions that are so long-lived because their major decay paths are M2 decays. Such levels and their decay chains play a significant role in various plasmas. Collisional-radiative modeling has to take them into account, and it can do so reliably, now that first benchmark measurements exist.

Fig. 9. Transition rate data (with error bars) and predictions for the $3s^2 3p\ ^2P^o_{3/2}$ level in the ground state of the Al-like ion Fe^{13+} (Fe XIV). Note how most calculational results agree within a close interval with each other, because they have been adjusted to match the experimental transition energy. The three older ab initio theoretical results scatter notably. The ab initio result presented by Huang is based on too few configurations to be expected to be reliable. The agreement of this result with experiment must be seen as fortuitous, because the same type of calculation has a grossly deviant result for Fe X (see ref. 143). The electrostatic ion trap measurement by Moehs and Church [65] caused some confusion, until the electron beam ion trap measurement by Beiersdorfer et al. at Livermore [67] settled the case. The latest calculation, by Vilkas and Ishikawa [144] is the first that obtains close matches with experiment for both line strength and transition energy using ab initio techniques. Meanwhile the Heidelberg electron beam ion trap group has also measured this rate [107, 140] and finds agreement with the LLNL electron beam ion trap result and with the trend of the predictions.

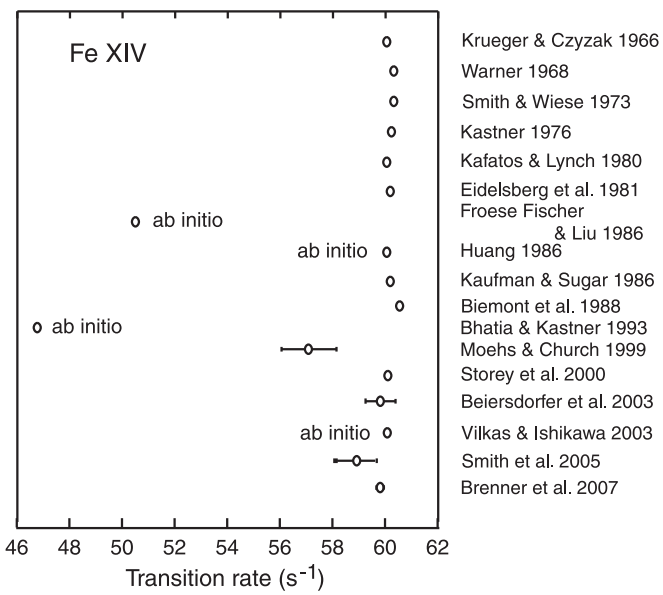

© 2008 NRC Canada

Table 3. Atomic lifetime results of electron beam ion trap measurements on many-electron ions with E1-forbidden decays (M1, E2, M2). The measurements were done at Gaithersburg (NIST), Livermore (LLNL), and Heidelberg (HD).

Ion	Level	Lifetime τ	Trap	Ref.	Comment
Al sequence					
Fe^{13+}	$3s^2 3p\ ^2P^o_{3/2}$	(16.74 ± 0.12) ms	LLNL EBIT	67	532 nm M1(E2)
		$(16.726^{+0.020}_{-0.010})$ ms	HD EBIT	140	
Si sequence					
Kr^{22+}	$3s^2 3p^2\ ^3P_2$	(5.7 ± 0.5) ms	NIST EBIT	90	384 nm M1
		(6.3 ± 0.3) ms	LLNL EBIT	93	
		(6.82 ± 0.1) ms	LLNL EBIT	95	
P sequence					
Kr^{21+}	$3s^2 3p^3\ ^2D^o_{5/2}$	(0.80 ± 0.03) ms	LLNL EBIT	97	345 nm M1
Ar sequence					
Kr^{18+}	$3s^2 3p^5 3d\ ^3P^o_2$	(2.20 ± 0.2) ms	LLNL EBIT	97	403 nm M1+M2
Kr^{18+}	$3s^2 3p^5 3d\ ^3F^o_2$	(4.2 ± 0.5) ms	LLNL EBIT	97	579 nm M1+M2
K sequence					
Kr^{17+}	$3s^2 3p^6 3d\ ^2D_{5/2}$	(22.7 ± 1.0) ms	LLNL EBIT	97	637 nm M1
Ca sequence					
Kr^{18+}	$3s^2 3p^6 3d^2\ ^3P_2$	(≈ 4.2) ms	LLNL EBIT	97	545 nm M1
Ti sequence					
Xe^{32+}	$3s^2 3p^6 3d^4\ ^5D_3$	(2.15 ± 0.14) ms	NIST EBIT	89	414 nm M1

Fig. 10. The lifetime of the $3s3p^2\ ^2D^o_{5/2}$ level in the ground configuration of P-like ions has been measured (with small error bars) at the TSR heavy-ion storage ring (data on Fe^{11+} and Co^{12+} [139]) and at the Livermore electron beam ion trap (Kr^{21+} [97]). The isoelectronic comparison with various calculations and tabulations shows that there is a wide scatter of the predictions, and that often the isoelectronic trend is also incorrectly predicted.

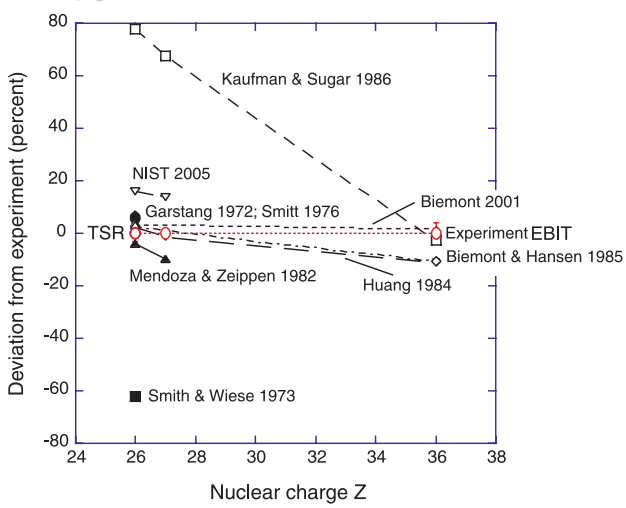

The atomic lifetime data on multielectron ions established at EBITs are summarized in Table 3.

5.4. Ti isoelectronic sequence

There are interesting atomic physics systems that appear to have useful applications but pose persistent challenges to theory. For example, there is an M1 fine-structure transition in the $3d^4$ ground configuration (which has many levels) of Ti-like heavy ions that happens to vary very little in wavelength over a wide range of nuclear charges. This peculiar behavior has been found in a theory search [145], which has led to searches for the lines in several EBIT laboratories. For more than 30 consecutive elements of the isoelectronic sequence, the line wavelength lies in the near ultraviolet, which is very advantageous for optics and low-noise detectors. At high Z, a decay branch to another level comes into play and gradually dominates, but the leftover branch was enough to permit measurments up to $Z = 83$ so far. A comparable system is being found in the $4d^4$ configuration, but there the wavelengths are longer (which is less convenient) and the ionization potentials are lower (which makes the ions less interesting as a probe of hot plasmas).

The situation with the Ti isoelectronic sequence is rather fortuitous for plasma diagnostics; an observational instrument could be optimized for a rather narrow wavelength range in the near UV and detect whether the Ti-like ion of a given seed element is present, immediately telling of the temperature (the electron temperature has to be high enough to produce the ion, but must not be so high as to destruct it by further ionization). The ionization potentials of the Ti-like ions range up to about 10 keV for U ($Z = 92$). The wavelength of this line has been measured for a great many ions of the isoelectronic sequence [146–148], and there also are rather many calculations. They happen to not quite match the experimental data, although some calculations from Japan come closer than all others to the experimental energy intervals (but these have not been reproduced elsewhere). However, there is an apparent discontinuity in the wavelength predictions for ions near $Z = 55$.

© 2008 NRC Canada

Fig. 11. Decay curve extracted from microcalorimeter observations of the M3 decay of the metastable $3d^9 4s\ ^3D_3$ level in the Ni-like ion Xe^{26+} [121], using a natural isotope mixture. All delayed emission photons in the interval 570 to 610 eV were used (the M3 decay is at 590 eV [151]). Assuming a single exponential decay, the decay data yield a lifetime result of (11.5 ± 0.5) ms [121]. Yao et al. [152] suggest that this decay curve may appear like a single exponential, but that it consists, in fact, of many components, because hyperfine interaction mixes the F levels. According to these calculations, all even isotopes contribute one decay component, ^{129}Xe contributes one more, and ^{131}Xe another three components. Adapted from ref. 121. Original figure copyright 2006 American Physical Society.

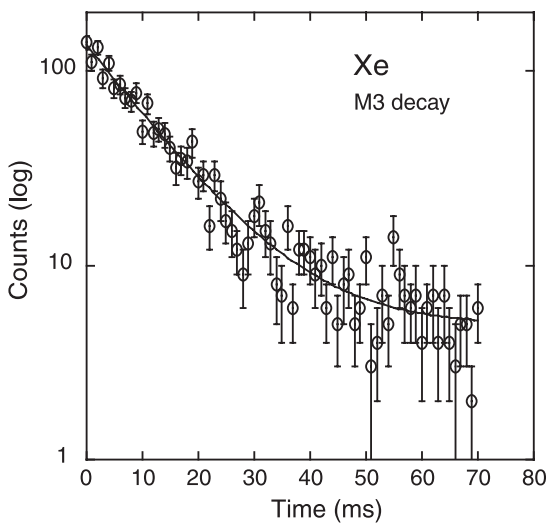

There is only a single lifetime measurement result on such a transition [89], and it agrees with various calculations within its 6% error bar. Further wavelength and lifetime measurements in this section of the isoelectronic sequence might help elucidate the exact position of the discontinuity and provide a check on the validity of the chosen wave functions in the same range [149]. Also, it should be possible to decrease the lifetime error bar considerably. In fact, a test to this effect at LLNL, using the aforementioned "stovepipe" instrument, looked quite promising, but there was not enough time yet to pursue this and eventually reach statistical reliability.

5.5. M3 transition rates

In a classical light source, only electric dipole transitions are being seen, because only these have transition rates that are higher than the collision frequencies in the light source medium. M1 and E2 transitions have transition rates that in light ions are many orders of magnitude lower, but, as we have seen, the progress in vacuum technology has made high vacua possible in which the collision frequencies are low enough so that such electric-dipole forbidden radiative transitions can be observed — they anyway can be observed in outer space. Higher multipole orders are expected to be even weaker (in low-Z ions), but their transition rates scale steeply with the transition energy (and thus effectively with the nuclear charge). Octupole transitions might seem exotic from a low-Z viewpoint, but interest was shown in them some time ago. E3 transitions in neutral atoms or singly charged ions (as well as hyperfine-induced transitions) are being studied for a role in atomic clocks, precisely because their transition rate is so low (and thus their upper level narrow); level lifetimes up to several years (measured by laser probing of excited trapped ions) are being considered.

Ni-like ions have a ground state with a closed $3d^{10}$ shell, and the lowest excited levels ($3d^9 4s$) cannot decay by electric dipole radiation. The lowest order multipole decay of the $J = 3$ level is by a magnetic octupole (M3) transition. M3 transitions have been seen brightly in the X-ray spectra of Ni-like Th and U [150] where the transition rates are very high and thus the level lifetimes very short. A practical lifetime measurement with an EBIT can be done somewhere in between, and the Livermore EBIT group has chosen Ni-like Xe^{26+} ions for this exercise.

A high-resolution EUV spectrometer with a (time-integrating) CCD detector was used to pinpoint the energy of the M3 transition in Ni-like Xe, and then a microcalorimeter was employed for time-resolved studies of the same transition in Ni-like Xe^{26+} [121]. In the measurements with the flat-field spectrograph, the M3 decay in the Ni-like Xe ion was indeed observed [151], but only as a weak line, because a long-lived level like this (predictions range from 14 to 19 ms) is also depopulated by the electron beam. Nevertheless, in two-dimensional spectra (energy versus time in the EBIT trapping cycle) this line showed up as the only one with a typical decay curve (Fig. 11). The Xe line was the only spectral feature with a decay curve time constant of the order of milliseconds (the measurement on natural Xe yields an apparent lifetime of 11.5 ± 0.5 ms). Corresponding data on Cs and Ba show the same significant deviation of theory from the experimental findings [121] (Table 4, Fig. 12), with the calculated values exceeding experiment by about 30 to 50%. The experimentally determined lifetimes make these levels slightly less density-sensitive than predicted. This is the first example of an atomic lifetime measurement using a microcalorimeter, and in this the new device has already proven its unique properties.

However, this is not the end of the story. Yao et al. [152], a group of Lund University, and Shanghai EBIT researchers have suggested that the decay rate difference between Livermore measurements and calculations for Xe (the considerable differences among the various calculations notwithstanding) might arise from hyperfine mixing. Natural xenon has many isotopes, and among them there are two that make up almost half the total abundance and have a nonzero nuclear spin and thus hyperfine structure. One of the hyperfine sublevels of $J = 3$ would remain unperturbed, but the others would mix with hyperfine sublevels of the $J = 2$ levels, resulting in F sublevels with individual lifetimes. For the isotope ^{129}Xe, which has a nuclear spin $I = 1/2$, there would be one level with a lifetime shortened by hyperfine mixing, whereas for ^{131}Xe (with a nuclear spin $I = 3/2$) there would be three. The LLNL EBIT group has since done experiments using pure even and odd Xe isotopes (^{132,129}Xe), and employing a large-solid angle, low spectral resolution detector [153]. The rather different shapes of the decay curves (Fig. 13) corroborate the claim that hyperfine mixing is important, and the actual results determine the M3/E2 HFS mixing with an uncertainty of only a few percent (Table 4).

© 2008 NRC Canada

Table 4. Atomic lifetime results of Livermore EBIT measurements on the M3 decay of the metastable $3d^94s\,^3D_3$ level in Ni-like ions. The first experiment [121] used a natural Xe isotope mixture. The original evaluations were based on the assumption of a single exponential decay component. For Xe, new experiments with individual even and odd isotopes have confirmed that hyperfine structure plays a role.

Ion	Lifetime τ	Comment	Ref.	Wavelength
Xe^{26+}	(11.5±0.5) ms	natural isotope mix	121	2.0 nm
	(2.7±0.1) ms	^{129}Xe $F = 5/2$	153	
	(15.1±0.5) ms	^{129}Xe $F = 7/2$	153	
	(15.06±0.24) ms	^{132}Xe	153	
Cs^{27+}	(8.2±2.0) ms	single odd isotope	121	1.9 nm
Ba^{28+}	(4.3±3.6) ms	natural isotope mix	121	1.8 nm

Fig. 12. Results of a microcalorimeter-based lifetime measurement (full symbols) of the metastable $3d^94s\,^3D_3$ level in Ni-like ions, compared with predictions by Safronova et al. [154], the only ones that are available for the isoelectronic sequence. (Figure adapted from ref. 121). Other atomic structure codes yield level lifetimes that are some 20% shorter, which is still off the experimental trend. We note that the measurement on Cs refers to a single isotope (with hyperfine structure), whereas Xe and Ba have several isotopes of zero and nonzero nuclear spin, respectively. None of the calculational results shown include the hyperfine structure. According to calculations by Yao et al. [152], hyperfine interaction mixes $3d^94s\,^3D_3$ and $^3D_2$ levels. Simulating a decay curve for a natural isotope mixture of Xe, Yao et al. can reproduce the experimental lifetime finding for Xe. A cleaner experimental procedure, a measurement with pure isotopes, is demonstrated in Fig. 13.

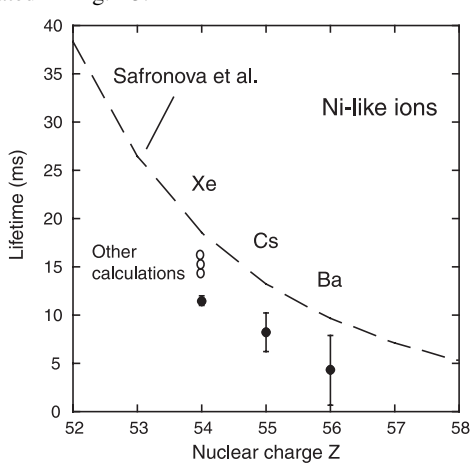

Hyperfine mixing evidently has a notable effect only on some very long-lived atomic level lifetimes, but they are exactly the ones of particular interest for some atomic clock schemes and in astrophysics!

The M3 decay of the $3d^94s\,^3D_3$ level is the most spectacular case of longevity in Ni-like ions. However, there also is the $3d^94s\,3D_2$ level with its E2 decay (the hyperfine mixing partner in the odd isotopes). The decay rate of this level is significantly higher than that of the $J = 3$ level, but orders of magnitude lower than those of the $J = 1$ levels (with M1 decays). Due to the steep Z scaling, the E2 decay rate should be measurable in ions like Ni-like Kr^{8+} (level lifetime about 6 μs [154]). The wavelength of this decay puts the transition into the EUV near 80 eV [154], and thus out of reach of the Livermore microcalorimeter. Instead, one might use a grating spectrograph (of, alas, much lower overall efficiency) with a time-resolving detector. A further challenge lies in the low ionization potential of such an ion that is difficult to produce without producing a wide range of ions in neighboring charge states at the same time, which would take possible signal away from the ion of interest.

Fig. 13. Decay curves extracted from proportional counter observations of Xe in SuperEBIT[3]. The experiment with a single even isotope (^{132}Xe, nuclear spin zero, no HFS) reveals a single radiative decay component of about 15 ms lifetime, and a decay curve tail that arises from charge exchange of trapped ions with the neutral gas that streams in. When using natural Xe with its about equal fractions of even and odd (nonzero nuclear spin) isotopes, the decay curve is more complex. Ni-like ions of several even and two odd Xe isotopes contribute components of five different lifetimes to this decay curve.
[3]E. Träbert, P. Beiersdorfer, G.V. Brown, H. Chen, J.H.T. Clementson, and D.B. Thorn. Manuscript in preparation.

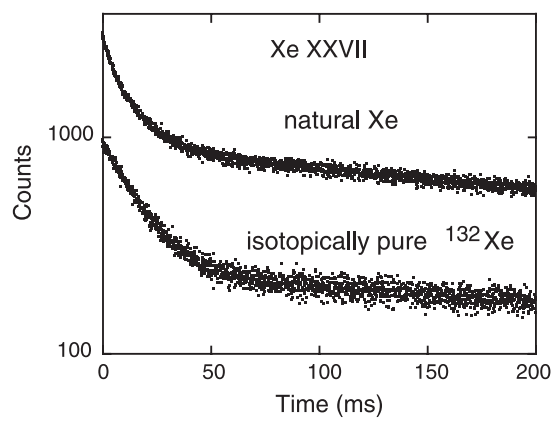

6. Conclusion and prospects

Tables 1–4 present a selection of the (long) atomic lifetime measurements that have been done with electron beam ion traps. All transitions are electric-dipole forbidden, with actual multipole orders ranging from M1 to M3. The ions studied belong

© 2008 NRC Canada

to isoelectronic sequences from He through Ni, that is, from few-electron ions, for which accurate measurements test details of the theoretical description, to many-electron ions that require quite different calculational techniques and that cannot yet be treated by theory with the reliability expected for few-electron ions. The published measurements reach from femtosecond lifetimes (by line broadening measuremenst) via microseconds to many milliseconds (by electronic timing), the wavelength ranges from the visible (several eV photon energy) to the X-ray range (near 2 keV so far). Having identified crucial measurement parameters like the ion loss rate due to charge exchange, the systematic errors are under good control for atomic level lifetimes up to a few dozen milliseconds. It appears quite feasible to extend this range to about 100 ms in the near future, to provide data that are helpful in terrestrial or astrophysical plasma diagnostics. The other important aspect are precision and accuracy. With the Heidelberg EBIT measurements on B-like Ar suggesting that theory may be incomplete on a fairly simple atomic system, there is a need to provide independent evidence of similar or even higher precision and reliability. On the "atomic lifetime scene", theory has not been challenged too seriously so far, but precision measurements — many of them on ion traps like a heavy-ion storage ring or electron beam ion traps — have begun to change the situation. The experimental data have identified reasonable and deficient lifetime calculations of a number of atomic systems, and with progress in measurement quality, the theoretical approximations that have been tried so far will be truly tested.

Looking farther ahead, the selective excitation of ions that are stored in the electron beam ion trap, by laser, XFEL, or synchrotron light pulses, has been suggested and is being pursued by several groups. A first demonstration of excitation by VUV light from a free electron laser (FLASH at Hamburg) has recently been achieved by the Heidelberg group [155]. This success opens a new window into atomic structure and dynamics, including a different option for precision lifetime measurements.

Acknowledgment

The author gratefully acknowledges travel support from the German Research Association (DFG) and appreciates, with thanks, the hospitality and support experienced at the Livermore EBIT laboratory. The LLNL EBIT lifetime experiments benefited from support in particular by P. Beiersdorfer, G.V. Brown, J.R. Crespo López-Urrutia, C.L. Harris, P.A. Neill, and S.B. Utter. The work at the University of California Lawrence Livermore National Laboratory was performed under the auspices of the US Department of Energy under Contract No. W-7405-Eng-48.

References

1. L.J. Curtis, R.T. Deck, and D.G. Ellis. Phys. Lett. **230A**, 330 (1997).
2. C. Rothe, S.I. Hintschich, and A.P. Monkman. Phys. Rev. Lett. A, **96**, 163601 (2006).
3. L.J. Curtis. Phys. Scr. **T8**, 77 (1984).
4. M.J. Vilkas and Y. Ishikawa. Phys. Rev. A, **68**, 012503 (2003).
5. E. Träbert. *In* Accelerator-based atomic physics - techniques and applications. *Edited by* S.M. Shafroth and J.C. Austin. American Institute of Physics, Washington. 1997. p. 567.
6. H. Cederquist, M. Kisielinski, and S. Mannervik. J. Phys. B, **16**, L479 (1983).
7. H. Cederquist, M. Kisielinski, S. Mannervik, and T. Andersen. J. Phys. B, **17** 1969 (1983).
8. D.A. Church. Phys. Rep. **228**, 254 (1993).
9. E. Träbert. Phys. Scr. **61**, 257 (2000).
10. E. Träbert. Phys. Scr. **T100**, 88 (2002).
11. E. Träbert. Can. J. Phys. **80**, 1481 (2002).
12. K.C. Steenbrugge, J.S. Kaastra, D.M. Crenshaw, S.B. Kraemer, N. Arav, I.M. George, D.A. Liedahl, R.L.J. van der Meer, F.B.S. Paerels, T.J. Turner, and T. Yaqoob. Astron. Astrophys. **434**, 569 (2005).
13. P. Beiersdorfer, A.L. Osterheld, J.H. Scofield, J.R. Crespo López-Urrutia, and K. Widmann. Phys. Rev. Lett. **80**, 3022 (1998).
14. I. Klaft, S. Borneis, T. Engel, B. Fricke, R. Grieser, G. Huber, T. Kühl, D. Marx, R. Neumann, S. Schröder, P. Seelig, and L. Völker. Phys. Rev. Lett. **73**, 2425 (1994).
15. T. Brage, P.L. Judge, and C.R. Proffitt. Phys. Rev. Lett. **89**, 281101 (2002).
16. S. Schippers, E.W. Schmidt, D. Bernhardt, D. Yu, A. Müller, M. Lestinsky, D.A. Orlov, M. Grieser, R. Repnow, A. Wolf. Phys. Rev. Lett. **98**, 033001 (2007).
17. S. Mrozowski. Zs. Phys. **108**, 204 (1940).
18. E.G. Myers, D.J.H. Howie, J.K. Thompson, and J.D. Silver. Phys. Rev. Lett. **76**, 4899 (1996).
19. R. Marrus, A. Simionovici, P. Indelicato, D.D. Dietrich, P. Charles, J.-P. Briand, K. Finlayson, F. Bosch, D. Liesen, and F. Parente. Phys. Rev. Lett. **63**, 502 (1989).
20. B.B. Birkett, J.P. Briand, P. Charles, D.D. Dietrich, K. Finlayson, P. Indelicato, D. Liesen, and R. Marrus, Phys. Rev. A, **47**, R2454 (1993).
21. A. Simionovici, B.B. Birkett, J.P. Briand, P. Charles, D.D. Dietrich, K. Finlayson, P. Indelicato, D. Liesen, and R. Marrus. Phys. Rev. A, **48**, 1695 (1993).
22. L.D. Huff and W.V. Houston. Phys. Rev. **36**, 842 (1930).
23. C. Jordan. Sol. Phys. **2**, 441 (1967).
24. C. Jordan. Mon. Not. R. Astron. Soc. **142**, 501 (1969).
25. C. Jordan. Sol. Phys. **21**, 381 (1971).
26. C. Jordan and P.L. Judge. Comm. At. Mol. Phys. **21**, 97 (1988).
27. C. Jordan. J. Opt. Soc. Am. B, **5**, 2252 (1988).
28. A.H. Gabriel. Mon. Not. R. Astron. Soc. **160**, 99 (1972).
29. D. Porquet, R. Mewe, J. Dubau, A.J.J. Raassen, and J.S. Kaastra. Astron. Astrophys. **376**, 1113 (2001).
30. M. Kafatos and J.P. Lynch. Astrophys. J. Suppl. Ser. **42**, 611 (1980).
31. J.P. Lynch and M. Kafatos. Astrophys. J. Suppl. Ser. **76**, 1169 (1991).
32. E. Hinnov. Nucl. Instrum. Meth. **202**, 381 (1982).
33. B. Denne and E. Hinnov. Phys. Scr. **35**, 811 (1987).
34. D.H. Menzel. Mem. Roy. Soc. Sci. Liege, **17**, 113 (1969).
35. R.H. Garstang. *In* Planetary nebulae. *Edited by* D.E. Osterbrock and C.R. O'Dell. Dordrecht. 1968. p. 143.
36. H.E. Mason, A.K. Bhatia, S.O. Kastner, W.M. Neupert, and M. Swartz. Sol. Phys. **92**, 199 (1984).

© 2008 NRC Canada

37. S. Suckewer and E. Hinnov. Phys. Rev. A, **20**, 578 (1979).
38. V. Kaufman and J. Sugar. J. Phys. Chem. Ref. Data, **15**, 321 (1986).
39. R. Fisher and S. Musman. Astrophys. J. **195**, 801 (1975).
40. M. Guhathakurta, R.R. Fisher, and R.C. Altrock. Astrophys. J. **414**, L145 (1993).
41. G. Wallerstein and E.W. Brugel. Astron. Astrophys. **197**, 182 (1988).
42. D.E. Osterbrock. Astrophys. J. **246**, 696 (1981).
43. B.E. Woodgate, H.S. Stockman, J.R.P. Angel, and R.P. Kirshner. Astrophys. J. **188**, L79 (1974).
44. B.E. Woodgate, J.R.P. Angel, and R.P. Kirshner. Astrophys. J. **200**, 715 (1975).
45. R.L. Lucke, B.E. Woodgate, J.L. Culhane, D.G. Socker, and J.C. Zarnecki. Astrophys. J. **228**, 763 (1979).
46. H. Itoh. Nature, **281**, 656 (1979).
47. R.L. Lucke, T.R. Gull, B.E. Woodgate, and D.G. Socker. Astrophys. J. **235**, 882 (1980).
48. L.W. Brown, B.E. Woodgate, and R. Petre. Astrophys. J. **334**, 852 (1988).
49. L.M. Hobbs. Astrophys. J. **284**, L47 (1984).
50. K. Anton, S. Wagner, and I. Appenzeller. Astron. Astrophys. **246**, L51 (1991).
51. U. Feldman. Phys. Scr. **63**, 276 (2001).
52. B.C. Fawcett and H.E. Mason. At. Data Nucl. Data Tables, **47**, 17 (1991).
53. D.A. Liedahl. *In* Atomic data needs for x-ray astronomy. *Edited by* M.A. Bautista, T.R. Kallman, and A.K. Pradhan. Goddard Space Flight Center, Greenbelt, Md. 2000. p. 151. (http://heasarc.gsfc.nasa.gov/docs/heasarc/atomic/)
54. E. Träbert, R. Hutton, and I. Martinson. Mon. Not. R. Astron. Soc. **227**, 27 (1987).
55. E. Träbert, P.H. Heckmann, R. Hutton, and I. Martinson. J. Opt. Soc. Am. B, **5**, 2173 (1988).
56. C. Jupén, R.C. Isler, and E. Träbert. Mon. Not. R. Astron. Soc. **264**, 627 (1993).
57. E. Träbert, M. Brandt, J. Doerfert, J. Granzow, P.H. Heckmann, J. Meurisch, I. Martinson, R. Hutton, and R. Myrnäs. Phys. Scr. **48**, 580 (1993).
58. E. Träbert. J. Phys. B: At. Mol. Opt. Phys. **29**, L217 (1996).
59. E. Träbert. Mon. Not. R. Astron. Soc. **297**, 399 (1998).
60. M. Eidelsberg, F. Crifo-Magnant, and C.J. Zeippen. Astron. Astrophys. Suppl. Ser. **43**, 455 (1981).
61. D.W. Savin, B. Beck, P. Beiersdorfer, S.M. Kahn, G.V. Brown, M.F. Gu, D.A. Liedahl, and J.H. Scofield. Phys. Scr. **T80**, 312 (1999).
62. J.K. Lepson, P. Beiersdorfer, G.V. Brown, D.A. Liedahl, S.B. Utter, N.S. Brickhouse, A.K. Dupree, J.S. Kaastra, R. Mewe, and S.M. Kahn. Astrophys. J. **578**, 648 (2002).
63. A.K. Bhatia and G.A. Doschek. At. Data Tables Nucl. Data Tables, **60**, 97 (1995).
64. A.K. Bhatia and S.O. Kastner. J. Quant. Spectrosc. Radiat. Transfer, **49**, 609 (1993).
65. D.P. Moehs and D.A. Church. Astrophys. J. **516**, L111 (1999).
66. E. Träbert, G. Gwinner, A. Wolf, E.J. Knystautas, H.-P. Garnir, and X. Tordoir. J. Phys. B: At. Mol. Opt. Phys. **35**, 671 (2002).
67. P. Beiersdorfer, E. Träbert, and E.H. Pinnington. Astrophys. J. **587**, 836 (2003).
68. S.J. Smith, A. Chutjian, and J.A. Lozano. Phys. Rev. A, **72**, 062504 (2005).
69. E. Träbert, P. Beiersdorfer, S.B. Utter, G.V. Brown, C.L. Harris, P.A. Neill, D.W. Savin, and A.J. Smith. Astrophys. J. **541**, 506 (2000).
70. D.P. Moehs and D.A. Church. Phys. Rev. A, **58**, 1111 (1998).
71. S.B. Utter, P. Beiersdorfer, J.R. Crespo López-Urrutia, and K. Widmann. Nucl. Instrum. Methods, A, **428**, 276 (1999).
72. J.V. Porto, I. Kink, and J.D. Gillaspy. Rev. Sci. Instrum. **71**, 3050 (2000).
73. V. Weisskopf and E. Wigner. Z. Phys. **63**, 54 (1933).
74. W. Heitler. The quantum theory of radiation. 3rd ed. Dover, Mineola, New York. 1984.
75. R.D. Cowan. The theory of atomic structure and spectra. University of California Press, Berkeley, Calif. 1981.
76. H.R. Griem. Spectral line broadening by plasmas. Academic Press, New York. 1974.
77. H.O. Di Rocco. J. Quant. Spectrosc. Radiat. Transfer, **92**, 231 (2005).
78. E.P. Petrov. J. Quant. Spectrosc. Radiat. Transfer, **103**, 272 (2007).
79. P. Beiersdorfer, A.L. Osterheld, V. Decaux, and K. Widmann. Phys. Rev. Lett. **77**, 5353 (1996).
80. P. Beiersdorfer, V. Decaux, S.R. Elliott, K. Widmann, and K. Wong. Rev. Sci. Instrum. **66**, 303 (1995).
81. P. Beiersdorfer, R.E. Olson, L. Schweikhard, P. Liebisch, G.V. Brown, J.R. Crespo López-Urrutia, C.L. Harris, P.A. Neill, S.B. Utter, and K. Widmann. AIP Conf. Proc. **500**, 626 (2000).
82. P. Beiersdorfer, A.L. Osterheld, V. Decaux, and K. Widmann. Phys. Rev. Lett. **77**, 5353 (1996).
83. A. Graf, P. Beiersdorfer, C.L. Harris, D.Q. Hwang, and P.A. Neill. *In* CP645, Spectral line shapes: Vol. 12. Proc. 16th ICSLS. *Edited by* C.A. Back. American Institute of Physics, Washington. 2002.
84. W.R. Johnson, D.R. Plante, and J. Sapirstein. *In* Advances of atomic, molecular and optical physics. Vol. 35. *Edited by* B. Bederson and H. Walther. Academic Press, San Diego. 1995. p. 255.
85. H.-D. Betz, F. Bell, H. Panke, G. Kalkoffen, M. Welz, and D. Evers. Phys. Rev. Lett. **33**, 807 (1974).
86. B.J. Wargelin, P. Beiersdorfer, and S.M. Kahn. Phys. Rev. Lett. **71**, 2196 (1993).
87. P. Beiersdorfer, L. Schweikhard, J. Crespo López-Urrutia, and K. Widmann. Rev. Sci. Instrum. **67**, 3818 (1996).
88. P. Beiersdorfer, B. Beck, St. Becker, and L. Schweikhard. Int. J. Mass Spectrom. Ion Proc. **157/158**, 1491 (1996).
89. F.G. Serpa, C.A. Morgan, E.S. Meyer, J.D. Gillaspy, E. Träbert, D.A. Church, and E. Takács. Phys. Rev. A, **55**, 4196 (1997).
90. F.G. Serpa, J.D. Gillaspy, and E. Träbert. J. Phys. B: At. Mol. Opt. Phys. **31**, 3345 (1998).
91. S.B. Utter, P. Beiersdorfer, J.R. Crespo López-Urrutia, and E. Träbert. Rev. Sci. Instrum. **70**, 288 (1999).
92. S.B. Utter, J.R. Crespo López-Urrutia, P. Beiersdorfer, and E. Träbert. Rev. Sci. Instrum. **73**, 3737 (2002).
93. E. Träbert, P. Beiersdorfer, S.B. Utter, and J.R. Crespo López-Urrutia. Phys. Scr. **58**, 599 (1998).
94. E. Träbert and P. Beiersdorfer. Rev. Sci. Instrum. **74** 2127 (2003).
95. E. Träbert, S.B. Utter, and P. Beiersdorfer. Phys. Lett. **272A**, 86 (2000).
96. E. Träbert, P. Beiersdorfer, E.H. Pinnington, and D.B. Thorn. Phys. Rev. A, **64**, 034501 (2001).

© 2008 NRC Canada

97. E. Träbert, P. Beiersdorfer, G.V. Brown, H. Chen, D.B. Thorn, and E. Biémont. Phys. Rev. A, **64**, 042511 (2001).
98. E. Träbert, P. Beiersdorfer, G. Gwinner, E.H. Pinnington, and A. Wolf. Phys. Rev. A, **66**, 052507 (2002).
99. J.R. Crespo López-Urrutia, J. Braun, G. Brenner, H. Bruhns, C. Dimopoulou, I.N. Draganić, D. Fischer, A.J. González-Martínez, A. Lapierre, V. Mironov, R. Moshammer, R. Soria Orts, H. Tawara, M. Trinczek, and J. Ullrich. J. Phys. B, Conf. Ser. **2**, 42 (2004).
100. I. Draganić, J.R. Crespo López-Urrutia, R. DuBois, S. Fritzsche, V.M. Shabaev, R. Soria Orts, I.I. Tupitsyn, Y. Zou, and J. Ullrich. Phys. Rev. Lett. **91**, 183001 (2003).
101. A. Volotka, D.A. Glazov, G. Plunien, V.M. Shabaev, and I.I. Tupitsyn. Eur. Phys. J. D, **38**, 293 (2006).
102. L. Yang, D.A. Church, S. Tu, and J. Jin. Phys. Rev. A, **50**, 177 (1994).
103. D.A. Church, D.P. Moehs, and M.I. Bhatti. Int. J. Mass Spectrom. **192**, 149 (1999).
104. T.V. Back, H.S. Margolis, P.K. Oxley, J.D. Silver, and E.G. Myers. Hyperfine Int. **114**, 203 (1998).
105. J.R. Crespo López-Urrutia, J. Braun, G. Brenner, H. Bruhns, C. Dimopoulou, I.N. Draganic, D. Fischer, A.J. González Mart'nez, A. Lapierre, V. Mironov, R. Moshammer, R. Soria Orts, H. Tawara, M. Trinczek, and J. Ullrich. J. Phys.: Conf. Ser. **2**, 42 (2004).
106. A. Lapierre, U.D. Jentschura, J.R. Crespo López-Urrutia, J. Braun, G. Brenner, H. Bruhns, D. Fischer, A.J. González-Martínez, Z. Harman, W.R. Johnson, C.H. Keitel, V. Mironov, C.J. Osborne, G. Sikler, R. Soria Orts, V. Shabaev, H. Tawara, I.I. Tupitsyn, J. Ullrich, and A. Volotka. Phys. Rev. Lett. **95**, 183001 (2005).
107. A. Lapierre, J.R. Crespo López-Urrutia, J. Braun, G. Brenner, H. Bruhns, D. Fischer, A.J. González-Martínez, V. Mironov, C.J. Osborne, G. Sikler, R. Soria Orts, H. Tawara, J. Ullrich, V.M. Shabaev, I.I. Tupitsyn, and A. Volotka. Phys. Rev. A, **73**, 052507 (2006).
108. E. Träbert, A. Wolf, J. Linkemann, and X. Tordoir. J. Phys. B: At. Mol. Opt. Phys. **32**, 537 (1999).
109. E. Träbert, G. Gwinner, A. Wolf, X. Tordoir, and A.G. Calamai. Phys. Lett. **264A**, 311 (1999).
110. P. Beiersdorfer, G.V. Brown, L. Hildebrandt, K.L. Wong, and R. Ali. Rev. Sci. Instrum. **72**, 508 (2001).
111. E. Träbert, P. Beiersdorfer, G.V. Brown, A.J. Smith, M.F. Gu, and D.W. Savin. Phys. Rev. A, **60**, 2034 (1999).
112. E. Träbert, P. Beiersdorfer, and S.B. Utter. Phys. Scr. **T80**, 450 (1999).
113. G.S. Stefanelli, P. Beiersdorfer, V. Decaux, and K. Widmann. Phys. Rev. A, **52**, 3651 (1995).
114. J.R. Crespo López-Urrutia, P. Beiersdorfer, D.W. Savin, and K. Widmann. Phys. Rev. A, **57**, 238 (1998).
115. P.A. Neill, E. Träbert, P. Beiersdorfer, G.V. Brown, C.L. Harris, A.J. Smith, S.B. Utter, and K.L. Wong. Phys. Scr. **62**, 141 (2000).
116. J.R. Crespo López-Urrutia, P. Beiersdorfer, and K. Widmann. Phys. Rev. A, **74** 012507 (2006).
117. G.W.F. Drake. Phys. Rev. A, **3**, 908 (1971).
118. C.D. Lin. Ph.D. thesis, Columbia University. 1975.
119. F.S. Porter, M.D. Audley, P. Beiersdorfer, K.R. Boyce, R.P. Brekosky, G.V. Brown, K.C. Gendreau, J. Gygax, S. Kahn, R.L. Kelley, C.K. Stahle, and A.E. Szymkowiak. Proc. SPIE, **4140**, 407 (2000).
120. F.S. Porter, G.V. Brown, K.R. Boyce, R.L. Kelley, C.A. Kilbourne, P. Beiersdorfer, H. Chen, S. Terracol, S.M. Kahn, and A.E. Szymkowiak. Rev. Sci. Instrum. **75**, 3772 (2004).
121. E. Träbert, P. Beiersdorfer, G.V. Brown, K.R. Boyce, R.L. Kelley, C.A. Kilbourne, F.S. Porter, and A. Szymkowiak. Phys. Rev. A, **73**, 022508 (2006).
122. P. Beiersdorfer, J.H. Scofield, and A.L. Osterheld. Phys. Rev. Lett. **90**, 235003 (2003).
123. P. Beiersdorfer, J. Scofield, G.V. Brown, H. Chen, E. Träbert, and J.K. Lepson. *In* Proceedings of the 2006 NASA Laboratory Astrophysics Workshop. *Edited by* P.F. Weck and V.H.S. Kwong. NASA Conf. Proc. CP-2006-214549. p. 120.
124. G. Breit and E. Teller. Astrophys. J. **91**, 215 (1940).
125. A.H. Gabriel and C. Jordan. Nature, **221**, 947 (1969).
126. H.T. Schmidt, P. Forck, M. Grieser, D. Habs, J. Kenntner, G. Miersch, R. Repnow, U. Schramm, T. Schüssler, D. Schwalm, and A. Wolf. Phys. Rev. Lett. **72**, 1616 (1994).
127. H.T. Schmidt. Ph.D. thesis, Aarhus. 1994.
128. H. Chen, P. Beiersdorfer, M.-F. Gu, L.A. Heeter, J.K. Lepson, D.A. Liedahl, K.L. Naranjo-Rivera, and E. Träbert. Astrophys. J. **611**, 598 (2004).
129. J.R. Crespo López-Urrutia, P. Beiersdorfer, K. Widmann, and V. Decaux. *In* Nineteenth international conference on the physics of electronic and atomic collisions – Scientific Program and Abstracts of Contributed Papers. *Edited by* J.B.A. Mitchell, J.W. McConkey, and C.E. Brion. ICPEAC, Whistler, BC. 1995. p. 589.
130. J. Doerfert, E. Träbert, A. Wolf, D. Schwalm, and O. Uwira. Phys. Rev. Lett. **78**, 4355 (1997).
131. M.H. Chen, K.T. Cheng, and W.R. Johnson. Phys. Rev. A, **64**, 042507 (2001).
132. T.K. Krueger and S.J. Czyzak. Astrophys. J. **144**, 1194 (1966).
133. M.W. Smith and W.L. Wiese. J. Phys. Chem. Ref. Data, **2**, 85 (1973).
134. S.O. Kastner. Sol. Phys. **46**, 179 (1976).
135. C. Froese Fischer and B. Liu. At. Data Nucl. Data Tables, **34**, 261 (1986).
136. M.E. Galavís, C. Mendoza, and C. Zeippen. Astron. Astrophys. Suppl. Ser. **131**, 499 (1998).
137. E. Charro, S. López-Ferrero, and I. Martín. J. Phys. B: At. Mol. Opt. Phys. **34**, 4243 (2001).
138. E. Träbert, G. Saathoff, and A. Wolf. J. Phys. B: At. Mol. Opt. Phys. **37**, 945 (2004).
139. E. Träbert, S. Reinhardt, J. Hoffmann, and A. Wolf. J. Phys. B: At. Mol. Opt. Phys. **39**, 945 (2006).
140. G. Brenner, J.R. Crespo López-Urrutia, Z. Harman, P.H. Mokler, and J. Ullrich. Phys. Rev. A, **75**, 032504 (2007).
141. E. Träbert, G. Gwinner, A. Wolf, E.J., Knystautas, H.-P. Garnir, and X. Tordoir. J. Phys. B: At. Mol. Opt. Phys. **35**, 671 (2002).
142. E. Träbert, A.G. Calamai, G. Gwinner, E.J. Knystautas, E.H. Pinnington, and A. Wolf. J. Phys. B: At. Mol. Opt. Phys. **36**, 1129 (2003).
143. E. Träbert. Astron. Astrophys. **415**, L39 (2004).
144. M.J. Vilkas and Y. Ishikawa. Phys. Rev. A, **68**, 012503 (2003).
145. U. Feldman, P. Indelicato, and J. Sugar. J. Opt. Soc. Am. B, **8**, 3 (1991).

© 2008 NRC Canada

146. J.V. Porto, I. Kink, and J.D. Gillaspy. Phys. Rev. A, **61**, 054501 (2000).
147. H. Watanabe1, D. Crosby, F.J. Currell, T. Fukami, D. Kato, S. Ohtani, J.D. Silver, and C. Yamada. Phys. Rev. A, **63**, 042513 (2001).
148. S.B. Utter, P. Beiersdorfer, and E. Träbert. Phys. Rev. A, **67**, 012508 (2003).
149. E. Biémont, E. Träbert, and C.J. Zeippen. J. Phys. B: At. Mol. Opt. Phys. **34**, 1941 (2001).
150. P. Beiersdorfer, A.L. Osterheld, J. Scofield, B. Wargelin, and R.E. Marrs. Phys. Rev. Lett. **67**, 2272 (1991).
151. E. Träbert, P. Beiersdorfer, G.V. Brown, S. Terracol, and U.I. Safronova. Nucl. Instrum. Meth. Phys. Res. B, **235**, 23 (2005)
152. K. Yao, M. Andersson, T. Brage, R. Hutton, P. Jönsson, and Y. Zou. Phys. Rev. Lett. **97**, 183001 (2006).
153. E. Träbert, P. Beiersdorfer, and G.V. Brown. Phys. Rev. Lett. **98**, 263001 (2007).
154. U.I. Safronova, A.S. Safronova, S.M. Hamasha, and P. Beiersdorfer. At. Data Nucl. Data Tables, **92**, 47 (2006).
155. S. Epp, J.R. Crespo López-Urrutia, G. Brenner, V. Mäckel, P.H. Mokler, R. Treusch, M. Kuhlmann, M.V. Yurkov, J. Feldhaus, J.R. Schneider, M. Wellhöfer, M. Martins, W. Wurth, and J. Ullrich, Phys. Rev. Lett. **98**, 183001 (2007).

© 2008 NRC Canada